Lis1 binding regulates force-induced detachment of cytoplasmic dynein from microtubules

Emre Kusakci[1], Zaw Min Htet[2], John P. Gillies[3], Samara L. Reck-Peterson[3,4,5], Ahmet Yildiz[1,2,6]

[1]Graduate Group in Biophysics, University of California, Berkeley, CA, USA.

[2]Department of Molecular and Cellular Biology, University of California, Berkeley, CA, USA.

[3]Department of Cellular and Molecular Medicine, University of California San Diego, La Jolla, CA, USA.

[4]Department of Cell and Developmental Biology, University of California San Diego, La Jolla, CA, USA

[5]Howard Hughes Medical Institute, Chevy Chase, MD, USA.

[6]Physics Department, University of California, Berkeley, CA, USA.

Abstract

Cytoplasmic dynein-1 (dynein) is an AAA+ motor that transports intracellular cargos towards the microtubule minus end. Lissencephaly-1 (Lis1) binds to the AAA+ ring and stalk of dynein's motor domain and promotes the assembly of active dynein complexes. Because Lis1 slows motility when it remains bound to dynein, dissociation of Lis1 may be a key step in the initiation of dynein-mediated transport. Using single-molecule and optical trapping assays, we investigated how Lis1 binding affects the motility and force generation of yeast dynein in vitro. We showed that Lis1 does not slow dynein motility by serving as a roadblock or tethering dynein to microtubules. Lis1 binding also does not affect the forces that stall dynein movement, but it induces prolonged stalls and reduces the asymmetry in force-induced detachment of dynein from microtubules. Mutagenesis of the Lis1 binding sites on dynein's stalk partially recovers this asymmetry but does not restore dynein velocity. We propose that Lis1 binding slows dynein motility by disrupting nucleotide-induced rearrangements within the AAA+ ring and that Lis1's interaction with dynein's stalk slows force-induced detachment of dynein from microtubules.

Cytoplasmic dynein-1 (dynein hereafter) is the primary motor responsible for motility and force generation towards the minus ends of microtubules[1]. Dynein transports membranous organelles, vesicles, mRNA, and unfolded proteins towards the nucleus, drives retrograde transport in neurons, and plays crucial roles in cell division[2]. Mutations that impair dynein function are linked to severe neurodegenerative and developmental disorders[3].

The dynein complex consists of the dynein heavy chain (DHC) and associated subunits (Fig. 1a). The tail domain of the DHC facilitates dimerization and recruits other subunits. The motor domain forms a catalytic AAA+ ring that connects to the tail via the linker domain and to the microtubule via a coiled-coil stalk[4, 5] (Fig. 1a). ATP hydrolysis in the AAA+ ring is coupled to the swinging motion of the linker at the surface of the ring, which powers minus-end-directed motility and generates force[6]. Nucleotide hydrolysis also controls the binding and release of the motor from the microtubule by altering the registry of the stalk coiled coils[7]. Isolated dynein adopts an autoinhibited "phi" conformation and exhibits diffusive or nonprocessive motility on microtubules[8-10]. Processive motility is activated when dynein forms the dynein-dynactin-adaptor complex with its cofactor dynactin and the coiled-coil domain of adaptor proteins that link dynein to its many cargos[11, 12].

Dynein-mediated transport also requires Lis1, which is the only known regulatory protein that directly binds to the dynein motor domain[13]. Heterozygous mutations in the *LIS1* gene lead to neuronal migration deficiency during embryonic brain development and cause severe neurodevelopmental disease, lissencephaly[14]. Lis1 consists of an amino-terminal dimerization domain and a carboxy-terminal WD40 β-propeller domain that binds to dynein's motor domain at two sites, one on dynein's AAA+ ring and the other on dynein's stalk (Fig. 1a)[13, 15, 16]. Studies in live cells showed that Lis1 is a required cofactor for recruitment of dynein to kinetochores, the nuclear envelope, and the cell cortex, and the initiation of dynein-mediated transport of a wide variety of cargos, including Rab6-vesicles, lysosomes, and ribonucleoprotein complexes (reviewed in[17]). However, Lis1 has been reported to be absent from moving dynein cargos[18-21], suggesting that it is not required for dynein motility.

Recent in vitro and in vivo studies have proposed that Lis1 facilitates the assembly of active dynein-dynactin-adaptor complexes by preventing dynein from adopting the phi conformation[22-25]. Unlike dynactin, Lis1 is not required for subsequent dynein motility, and it appears to dissociate from most dynein complexes during or after the activation of processive motility[22, 23]. Dissociation of Lis1 may be a key step in dynein activation because the comigration of Lis1 substantially reduces the velocity of dynein complexes in vitro[22], and enhancing the affinity of dynein for Lis1 leads to defects in nuclear migration in the budding yeast, *S. cerevisiae*[26]. Several models have been proposed to explain how Lis1 binding pauses or slows down dynein motility. In vitro studies reported that Lis1 binding increases dynein's microtubule-binding affinity[13, 27-29]. Cryo-electron microscopy of Lis1-bound to dynein at the AAA+ site suggested that Lis1 clamps multiple AAA subunits together, trapping dynein in a conformation with high microtubule binding affinity, and possibly preventing rearrangements of the AAA subunits needed to switch to the low affinity conformation[16]. In addition, Lis1 binding to dynein has been proposed to inhibit or slow dynein motility by blocking the powerstroke of its linker domain[27], or by tethering dynein to the microtubule[24]. Lis1 was also shown to interact with the coiled-coil stalk of dynein when the AAA3 site is trapped in the ATP-bound state, and this interaction induces a lower microtubule affinity state[15]. Structure-guided mutations showed that the Lis1-stalk interaction is important for the localization of dynein to the cortex of yeast cells[15, 16].

However, it remains to be determined how the Lis1-stalk interaction affects the mechanism of dynein motility.

In this study, we used single-molecule imaging and optical trapping to investigate how Lis1 binding affects the motility and force generation of *S. cerevisiae* cytoplasmic dynein. Similar to mammalian dynein, Pac1 (the Lis1 homolog in *S. cerevisiae*, "Lis1" hereafter) binding to yeast dynein prevents it from adopting the phi confirmation, and mutants that cannot form the phi conformation partially rescue dynein function in yeast lacking Lis1[24]. Unlike mammalian dynein, yeast dynein is processive in the absence of dynactin and a cargo adaptor[30], and it has similar stepping and force generation properties to active mammalian dynein-dynactin-adaptor complexes[31-35]. Therefore, yeast dynein serves as a simpler model to investigate how Lis1 binding affects the intrinsic motility and force generation properties of dynein. Consistent with previous observations[13, 27-29], here we find that Lis1 binding slows dynein motility, induces longer run times on microtubules in unloaded conditions, and results in slower microtubule detachment of dynein under hindering forces. We find that Lis1 weakly interacts with the microtubule lattice, but that this interaction does not slow dynein motility. Our optical trapping measurements show that Lis1 does not reduce the dynein stall force, but rather decreases the asymmetry in velocity of dynein from the microtubule under force. Mutations that disrupt Lis1's interactions with dynein's stalk partially restore the asymmetric detachment of dynein from microtubules in the presence of Lis1. These observations provide new insight into the mechanism of dynein regulation by Lis1.

Results

Lis1 binding stoichiometrically slows down dynein motility

We expressed the full-length DHC (*DYN1*) with an amino-terminal GFP tag and a carboxy-terminal HaloTag from its endogenous locus in an *S. cerevisiae* strain lacking the genes encoding Lis1 (*PAC1*), the Lis binding protein, NudEL (*NDL1*), and the p150 subunit of dynactin (*NIP100*, Extended Data Table 1). The DHC co-purified with the endogenous dynein light intermediate chain (Dyn3), light chain (Dyn2), and intermediate chain (Pac11)[30]. We monitored the motility of this endogenously expressed complex (hereafter dynein) on surface-immobilized microtubules in the presence and absence of Lis1 using total-internal reflection fluorescence (TIRF) microscopy (Fig. 1a). Consistent with a previous report[13], GFP-dynein moved at 112 ± 5 nm s^{-1} (mean ± s.e.m.) in the absence of Lis1, and unlabeled Lis1 slowed dynein motility by 77% with a dissociation constant (K_D) of 17.9 ± 2.5 nM (±s.e., Fig. 1b,c). Lis1 also increased the run time of individual motors, indicating that Lis1 increases the microtubule-binding affinity of dynein (Fig. 1d).

To determine how many Lis1 dimers can bind to a dynein dimer, we separately labeled two different batches of Lis1 with TMR and LD655 dyes. We then monitored the colocalization of TMR-Lis1 and LD655-Lis1 with moving GFP-dynein in a three-color TIRF assay. In this assay, colocalization of dynein with a single color of Lis1 might be due to one or two Lis1 dimers bound per dynein, whereas colocalization of both dyes with the GFP signal would ensure that two Lis1 dimers are bound to dynein. We observed either LD655-Lis1 or TMR-Lis1 translocating together with dynein on microtubules at similar colocalization percentages (14% each; Fig. 1e, Supplementary Movie 1). A small fraction (1%) of GFP-dynein motors colocalized with LD655- and TMR-Lis1 simultaneously, suggesting that a single dynein motor can recruit two Lis1 dimers (Fig. 1e,f), but this occurred rarely in our assay conditions[36]. Similar to mammalian dynein-

dynactin-adaptor complexes[22, 23], yeast dynein motors that colocalized with a single color of Lis1 moved slower (41 ± 1 nm s^{-1}) than motors that did not colocalize with Lis1 (110 ± 1 nm s^{-1}). When dynein co-localized with two Lis1 dimers, its velocity was further reduced (21 ± 4 nm s^{-1}) and its run time was further increased (Fig. 1f, Extended Data Fig. 1a). We also observed that transient binding of Lis1 paused or slowed dynein, whereas unbinding of Lis1 restored dynein's velocity (Fig. 1g, Extended Data Fig. 1b, Supplementary Movie 2). The velocity of dynein motors not colocalizing with Lis1 was similar to the dynein velocity when there was no Lis1 in the chamber (Fig. 1h). Therefore, Lis1 slows dynein motility only when it is directly bound to the motor, and the presence of excess Lis1 in the chamber does not affect dynein movement.

Previously, we showed that human Lis1 facilitates the recruitment of two dyneins to the dynactin-adaptor complex by opening dynein's autoinhibited phi-conformation[22, 23]. It is also possible that a Lis1 dimer can simultaneously bind to the motor domains of two dynein dimers (Fig. 1i) and recruit them together to the dynactin-adaptor complex. To test whether yeast Lis1 can simultaneously bind two dynein dimers, we differentially labeled two batches of dynein with LD555 and LD655 dyes and monitored their comigration on microtubules in the presence or absence of Lis1. Because the yeast strain we purify endogenous dynein from lacks the *NIP100* gene, a functional dynactin complex should not be present in our assays, and colocalization of two dyneins could only be mediated by Lis1. In the absence of Lis1, we observed less than 1% colocalization between dynein labeled with LD555 and LD655. The presence of Lis1 led to a marginal increase in colocalization between the differentially labeled dyneins, but these events were extremely rare (2%, Fig. 1i), suggesting that Lis1 does not effectively crossbridge two dyneins.

Lis1's interaction with the microtubule does not affect dynein velocity

Unlike mammalian Lis1[22, 23], yeast Lis1 has been reported to interact with microtubules[24]. Because the concentration of Lis1 scaled with Lis1's ability to reduce dynein velocity, the authors proposed that yeast Lis1 slows dynein by binding both dynein and the microtubule[24]. This tethering model requires that 1) either one Lis1 β-propeller in a Lis1 dimer interacts with dynein and the other with the microtubule, or 2) a single Lis1 β-propeller interacts simultaneously with both dynein and microtubule (Fig. 2a). The first model predicts that Lis1 monomers would not affect dynein's velocity. To test this, we measured the velocity of dynein in the presence of either wild-type Lis1 dimer ($Lis1^{WT}$) or monomeric Lis1 lacking its amino-terminal dimerization domain ($Lis1^{monomer}$)[13]. We observed that both dimers and monomers of Lis1 slowed dynein motility in a dose-dependent manner[13] (Fig. 2b). Thus, if Lis1 crosslinks dynein to microtubules, it must do so in the context of a monomer, with one face of Lis1 interacting with dynein and a different one interacting with microtubules.

The second model predicts that mutants that disrupt Lis1 binding to dynein would not disrupt Lis1 microtubule binding as the interfaces involved must be different. To test this, we characterized how Lis1 interacts with microtubules in vitro. As previously reported[24], $Lis1^{WT}$ decorates microtubules in 50 mM KAc (Fig. 2c). Lis1 maintained microtubule-binding when the carboxy-terminal tails of tubulin were cleaved by subtilisin treatment (Fig. 2d, Extended Data Fig. 2a). However, there was little to no microtubule decoration of Lis1 at a physiologically relevant salt concentration (150 mM KAc; Fig. 2c). We next used Lis1 mutants where a single ($Lis1^{R378A}$) or five ($Lis1^{5A}$) positively charged residues in Lis1's β-propeller domain were mutated to alanine. These mutations disrupt Lis1's binding to dynein's AAA+ ring (Extended Data Fig. 2b)[27]. Unlike $Lis1^{WT}$, $Lis1^{R378A}$ and $Lis1^{5A}$ were unable to decorate microtubules in 50 mM KAc

(Fig. 2e, Extended Data Fig. 2c-f). Lis1^{5A} also did not bind to microtubules in microtubule pelleting assays (Extended Data Fig. 2g), indicating that a Lis1 monomer would not be capable of crosslinking dynein to microtubules. We conclude that Lis1 interacts with the microtubule lattice primarily through electrostatic interactions between negatively charged microtubules and basic amino acids at the dynein-interacting surface of Lis1's β-propeller domain. However, this interaction is not strong enough to sustain microtubule binding in physiologically-relevant salt concentrations, consistent with the lack of microtubule colocalization of Lis1 in yeast cells[26].

Unlike our observations (Fig. 1h), Marzo et al. reported that the presence of Lis1 is sufficient to reduce the velocity of dynein motors that do not comigrate with Lis1[24]. This observation is inconsistent with the tethering model, which requires the comigration of Lis1 to slow dynein motility. Alternatively, Lis1 may serve as a static obstacle against dynein motility on the microtubule surface, akin to microtubule-associated proteins (MAPs)[37]. Because all dyneins would encounter microtubule-bound Lis1, this model predicts a similar reduction in velocity for dyneins that comigrate with Lis1 and those that are not bound to Lis1[24]. We pre-decorated microtubules with excess Lis1 with no added salt and washed away free Lis1 from the chamber (Extended Data Fig. 2h). The velocity of dynein on Lis1-decorated microtubules was similar to its velocity on undecorated microtubules (Fig. 2f, Supplementary Movies 3 and 4), demonstrating that microtubule decoration of Lis1 does not substantially slow dynein motility along these tracks.

To understand how Lis1 might slow motility without comigrating with dynein, we purified dynein from the *S. cerevisiae* strain used by Marzo et al.[24], which overexpresses DHC and each of its associated chains under the galactose promoter (hereafter dynein$_{Gal}$). Similar to dynein expressed using the endogenous promoter (Fig. 1), dynein$_{Gal}$ had an increased run length and run time when colocalized with Lis1 (Extended Data Figs. 3-5). However, dynein$_{Gal}$ motors moved significantly slower whether or not they colocalized with Lis1 in the chamber (Extended Data Fig. 4d), as reported[24]. The reduction in dynein$_{Gal}$ velocity was not due to decoration of the microtubule surface by Lis1, because Lis1 addition slowed dynein$_{Gal}$ even when it did not decorate microtubules under physiological salt (150 mM; Extended Data Fig. 3). We next introduced or removed Lis1 from the chamber while recording dynein$_{Gal}$ motility. Introducing Lis1 into the chamber did not alter the velocity of dynein$_{Gal}$ motors that were already moving along the microtubule at the time Lis1 was added (Extended Data Fig. 6a-c). Likewise, the removal of free Lis1 from the chamber failed to recover dynein$_{Gal}$ velocity (Extended Data Fig. 6c). While the underlying mechanism remains unclear, the differences between the Lis1-mediated regulation of dynein subunits expressed under their endogenous promoters and dynein$_{Gal}$ may be related to different stoichiometries of the dynein-associated chains in purified complexes or the tendency of dynein$_{Gal}$ to aggregate after purification[24].

Lis1 does not affect dynein stall force

We next investigated whether Lis1 binding slows dynein motility by interfering with the swinging motion of the linker at the surface of the ring, as previously proposed[27]. Because the linker drives the force-generating powerstroke of dynein, this model predicts that Lis1 binding reduces the ability of dynein to walk against hindering forces. To test this possibility, we returned to using the full-length dynein complex expressed under endogenous promoters and measured the stall force of GFP-dynein in the presence and absence of excess (300 nM) Lis1 using an optical trap (Fig. 3a). In the absence of Lis1, dynein stalled at 3.8 ± 0.1 pN (mean ± s.e.m., N = 116 stalls) and remained attached to the microtubule for 14.6 ± 0. 8 s (mean ± s.e.m.) before the bead snapped back to the trap center[33] (Fig. 3b,c). The stall force was unaltered

by Lis1 addition (3.8 ± 0.1 pN, N = 126 stalls; Fig. 3b,c), suggesting that Lis1 does not disrupt the force-generating powerstroke of the linker. However, the Lis1 addition resulted in a 70% increase in the duration of the stalls (24.7 ± 0.9 s, p = 0.018, Kolmogorov-Smirnov test), indicating that Lis1 reduces the microtubule detachment rate of dynein under hindering forces (Fig. 3d). Unlike full-length dynein, Lis1 binding reduced the stall force of tail-truncated GST-dimerized dynein (GFP-GST-Dyn_{331kDa} and GFP-GST-Dyn_{314kDa}) constructs[33, 38], suggesting that artificial dimerization of the linkers at the exit of the ring introduces a steric obstacle against their swinging motion when Lis1 is present on the outer surface of the ring (Extended Data Fig. 7). However, Lis1 binding does not affect the force generation of full-length dynein, presumably because the longer length of the full-length dynein tails has greater flexibility compared to the truncated dynein constructs used by Toropova et al.[27].

Lis1 reduces the asymmetry in force-induced detachment of dynein

Because Lis1 increases the microtubule affinity of dynein (Fig. 1)[13, 15, 16], we also tested whether Lis1 binding slows dynein motility by altering the detachment kinetics of dynein from the microtubule. Nucleotide hydrolysis in dynein's AAA+ ring controls its microtubule affinity by altering the registry of the stalk coiled coils[39-41]. The stalk sliding mechanism is also sensitive to external forces, such that dynein releases quickly from the microtubule and moves substantially faster when it is pulled in the assisting direction (towards the minus-end of microtubules), but it strongly resists backward movement when pulled in the hindering direction[33, 39]. If Lis1 binding interferes with this mechanism, we anticipated that the addition of Lis1 would reduce the asymmetry in the force-induced velocity of dynein. To test this prediction, we measured the velocity of dynein motors when they were subjected to constant forces in assisting and hindering directions using a force-feedback controlled trap. Dynein responded asymmetrically to external forces in the absence of Lis1 and its force-velocity (F-V) behavior in 2 mM ATP could be explained by the asymmetric potential barrier for the release of the motor from the microtubule[41] (Fig. 4a). The addition of 300 nM Lis1 reduced dynein velocity when the motor was being pulled in both directions (Fig. 4b). The velocity was reduced more substantially under assisting forces than under hindering forces (Fig. 4c,d), resulting in a reduced asymmetry in the F-V behavior of dynein in the presence of Lis1.

We reasoned that Lis1 binding may reduce the asymmetry in F-V by interfering with either the linker swing or the stalk sliding mechanisms of the dynein motor domain. To distinguish between these possibilities, we repeated the F-V measurements in the absence of ATP. The swinging motion of the linker is strictly coupled to the ATP hydrolysis cycle, whereas the registry of the stalk coiled-coils can be altered by external force even in the absence of ATP[40]. Similar to the ATP condition, Lis1 addition decreased dynein velocity when the motor was pulled in both directions and the decrease in velocity was more substantial when the motor was pulled in the assisting direction in the absence of ATP (Fig. 5a,b). These results suggest that Lis1 binding slows the detachment of dynein from microtubules by interfering with the stalk sliding mechanism.

Recently, we have shown that Lis1 stably interacts with a second binding site at the base of dynein's stalk when the AAA3 site of dynein is trapped in the ATP-bound state[15]. To test whether this Lis1-stalk interaction might be responsible for Lis1's ability to reduce the asymmetry in force-induced detachment of dynein from microtubules, we performed F-V measurements using a dynein mutant, in which three Lis1-interacting residues on its stalk were replaced with alanine ($dynein^{EQN}$, purified from yeast expressing dynein and its subunits from their endogenous promoters)[15]. We first confirmed that $dynein^{EQN}$ motility is slowed down by Lis1, albeit with a ~3-fold higher K_D (54 ±10 nM, ±s.e.) compared to that for wild-type

(WT) dynein[15] (Extended Data Fig. 8a,b). Similar to WT dynein, the binding of two Lis1 dimers further slowed dynein^{EQN} motility (Extended Data Fig. 8c,d). In the absence of Lis1, dynein^{EQN} also had similar stall force, but lower stall durations relative to WT dynein ($p = 0.03$, Kolmogorov-Smirnov test, Extended Data Fig. 8e-g). To determine how Lis1 affects stall force and F-V behavior of dynein^{EQN}, we used higher concentrations of Lis1 (900 nM) to compensate for dynein^{EQN}'s lower affinity for Lis1[15]. The addition of Lis1 resulted in only minor changes in the stall force and stall time of dynein^{EQN} (Extended Data Fig. 8e-g). Thus, the mutagenesis of the stalk interaction site of Lis1 does not abrogate its ability to induce a high microtubule affinity for dynein. However, unlike WT dynein, the addition of Lis1 did not reduce the asymmetry of dynein^{EQN}'s F-V behavior (Fig. 6 and Extended Data Fig. 9). Collectively, these results show that the Lis1-ring interaction is primarily responsible for the reduction of dynein velocity in Lis1-bound dynein and that the Lis1-stalk interaction reduces the asymmetry in force-induced detachment of dynein from the microtubule.

Discussion

Lis1 is a required cofactor for the initiation of dynein-mediated transport, but it needs to dissociate from the dynein complex to enable rapid transport of intracellular cargos[22-24]. In this study, we used single-molecule imaging to test the models that describe how Lis1 slows dynein motility when it remains bound to the dynein motor domain[13, 24, 27, 42]. We also performed optical trapping studies of active dynein complexes in the presence of Lis1 to understand how Lis1 binding affects force generation and force response of dynein. We showed that Lis1 binding does not affect the dynein stall force, indicating that the linker can perform its force-generating powerstroke when Lis1 is bound to the AAA+ ring. This result is consistent with the ability of dynein motors to walk processively, albeit at lower speeds, when colocalized with Lis1[22], whereas disrupting the linker swing mechanism fully abrogates the motility[43, 44]. We also showed that Lis1's interaction with the microtubule at low salt is not primarily responsible for slower motility, because Lis1 does not bind microtubules but still slows down dynein motility under physiological salt. Furthermore, decoration of the microtubule surface with Lis1 does not serve as an efficient obstacle against dynein motility, because dynein motors walk on these microtubules at full speed.

We observed that dynein moves slowly and runs on microtubules for a longer time when it colocalizes with a single Lis1, and its velocity decreases while its run time increases further when colocalized with two Lis1s. Lis1-bound dynein also persists against microtubule detachment for longer durations under hindering forces and moves slower under both assisting and hindering forces. Consistent with previous reports[13, 15, 16], these results indicate that Lis1 binding increases the microtubule binding affinity of dynein. Mutagenesis of the Lis1 interaction site on dynein's stalk in dynein^{EQN} did not recover dynein velocity, demonstrating that Lis1's interaction with the AAA+ ring is primarily responsible for slower movement[15, 16]. These results are consistent with a model in which Lis1 binding to the AAA+ ring prevents nucleotide-induced rigid body motions of the AAA+ subunits and traps the AAA+ ring in the high microtubule affinity conformation[15], resulting in a slower velocity.

Our optical trapping measurements provide evidence that Lis1 restricts the registry shift of the stalk coiled coils under external forces. Without Lis1, the dynein stalk switches from the strongly-bound to the weakly-bound registry when dynein is subjected to assisting forces but remains in a strongly-bound registry under hindering forces[40]. Lis1 binding slows WT dynein speed in both assisting and hindering forces, but it has a more profound effect in limiting the acceleration of dynein under assisting forces. These results indicate

that Lis1 binding may prevent dynein's stalk switching from the α registry to a registry with lower affinity. The Lis1 binding to dynein's stalk may restrict the registry shift of the coiled coils because Lis1 is less effective in reducing the speed of dynein motility under assisting forces when the stalk residues that interact with Lis1 were replaced with alanine.

We previously showed that Lis1 stably interacts with dynein's stalk and reduces microtubule affinity when the AAA3 site of dynein is unable to hydrolyze ATP and trapped at the ATP-bound state[15]. If the Lis1-stalk interaction also reduces microtubule affinity when the AAA3 site freely binds and hydrolyzes ATP, mutagenesis of the Lis1 interaction site on dynein's stalk would result in a more substantial reduction in velocity in the presence of external force. However, we observed that Lis1 is less effective in reducing the speed of dynein^{EQN} velocity under assisting forces, indicating that the Lis1-stalk interactions lead to an overall increase in microtubule affinity of WT dynein as it walks along the microtubule. Future structural and mechanistic work will be required to investigate whether Lis1 interacts with the stalk at different states of the dynein mechanochemical cycle and how these interactions regulate the microtubule affinity of the motor.

Recent studies in fungi showed that Lis1-mediated activation is required for dynein function[24, 25]. However, the dynein mutant that cannot adopt the phi conformation fails to fully rescue the deletion of Lis1 in *Aspergillus nidulans*[25], indicating that Lis1 may have additional regulatory roles, such as trapping the stalk coiled-coils in the high-affinity state when it remains bound to the motor domain. Lis1 may promote a high microtubule affinity state when dynein anchors large organelles to the microtubule network or pulls on astral microtubules during cell division[36, 45, 46]. Alternatively, a Lis1-mediated increase in microtubule affinity may contribute to the proper assembly of dynein with dynactin and an activating adaptor on the microtubule. In this scheme, Lis1 remains bound until an activating adaptor triggers its release from dynein during or after the assembly of the complex[45, 47], its dissociation initiates dynein-driven transport. Future studies are required to determine whether the association and dissociation of Lis1 from dynein are regulated in different cellular contexts.

Author Contributions: E.K., S.R.P., and A.Y. conceived the study and designed the experiments. Z.M.H. generated the yeast constructs for dynein and Lis1. E.K. purified the proteins, performed all single-molecule experiments, and analyzed all the data. J.P.G. performed experiments on monomeric Lis1. E.K., S.R.P., and A.Y. wrote the manuscript. All authors read and revised the manuscript.

Acknowledgments: We thank S. Can, M. ElShenawy, L. S. Ferro, J. T. Canty, and other members of the Yildiz and Reck-Peterson laboratories for helpful discussions, and S. M. Markus for sharing the yeast strain that expresses dynein$_{Gal}$. This work was supported by grants from the National Institute of General Medical Sciences (GM094522, AY), the National Science Foundation (MCB-1617028 and MCB-1055017, AY), and the Fellowship of the Ministry of Education of the Turkish Republic (E.K.). S.R.P. is a Howard Hughes Medical Institute Investigator and also supported by the National Institutes of Health (1R35GM141825).

Competing interests: The authors declare no competing interests.

References

1. Canty, J.T., Tan, R., Kusakci, E., Fernandes, J. & Yildiz, A. Structure and Mechanics of Dynein Motors. *Annual review of biophysics* **50**, 549-574 (2021).
2. Reck-Peterson, S.L., Redwine, W.B., Vale, R.D. & Carter, A.P. The cytoplasmic dynein transport machinery and its many cargoes. *Nature reviews. Molecular cell biology* **19**, 382-398 (2018).
3. Guedes-Dias, P. & Holzbaur, E.L.F. Axonal transport: Driving synaptic function. *Science* **366** (2019).
4. Carter, A.P., Cho, C., Jin, L. & Vale, R.D. Crystal structure of the dynein motor domain. *Science* **331**, 1159-1165 (2011).
5. Kon, T. *et al.* The 2.8 A crystal structure of the dynein motor domain. *Nature* **484**, 345-350 (2012).
6. Can, S., Lacey, S., Gur, M., Carter, A.P. & Yildiz, A. Directionality of dynein is controlled by the angle and length of its stalk. *Nature* **566**, 407-410 (2019).
7. Kon, T. *et al.* Helix sliding in the stalk coiled coil of dynein couples ATPase and microtubule binding. *Nature structural & molecular biology* **16**, 325-333 (2009).
8. Torisawa, T. *et al.* Autoinhibition and cooperative activation mechanisms of cytoplasmic dynein. *Nature cell biology* **16**, 1118-1124 (2014).
9. Trokter, M., Mucke, N. & Surrey, T. Reconstitution of the human cytoplasmic dynein complex. *Proceedings of the National Academy of Sciences of the United States of America* **109**, 20895-20900 (2012).
10. Zhang, K. *et al.* Cryo-EM Reveals How Human Cytoplasmic Dynein Is Auto-inhibited and Activated. *Cell* **169**, 1303-1314 e1318 (2017).
11. McKenney, R.J., Huynh, W., Tanenbaum, M.E., Bhabha, G. & Vale, R.D. Activation of cytoplasmic dynein motility by dynactin-cargo adapter complexes. *Science* **345**, 337-341 (2014).
12. Schlager, M.A., Hoang, H.T., Urnavicius, L., Bullock, S.L. & Carter, A.P. In vitro reconstitution of a highly processive recombinant human dynein complex. *The EMBO journal* **33**, 1855-1868 (2014).
13. Huang, J., Roberts, A.J., Leschziner, A.E. & Reck-Peterson, S.L. Lis1 acts as a "clutch" between the ATPase and microtubule-binding domains of the dynein motor. *Cell* **150**, 975-986 (2012).
14. Reiner, O. *et al.* Isolation of a Miller-Dieker lissencephaly gene containing G protein beta-subunit-like repeats. *Nature* **364**, 717-721 (1993).
15. DeSantis, M.E. *et al.* Lis1 Has Two Opposing Modes of Regulating Cytoplasmic Dynein. *Cell* **170**, 1197-1208 e1112 (2017).
16. Gillies, J.P. *et al.* Structural basis for cytoplasmic dynein-1 regulation by Lis1. *eLife* **11** (2022).
17. Markus, S.M., Marzo, M.G. & McKenney, R.J. New insights into the mechanism of dynein motor regulation by lissencephaly-1. *eLife* **9** (2020).
18. Egan, M.J., Tan, K. & Reck-Peterson, S.L. Lis1 is an initiation factor for dynein-driven organelle transport. *J Cell Biol* **197**, 971-982 (2012).
19. Lee, W.L., Oberle, J.R. & Cooper, J.A. The role of the lissencephaly protein Pac1 during nuclear migration in budding yeast. *J Cell Biol* **160**, 355-364 (2003).
20. Lenz, J.H., Schuchardt, I., Straube, A. & Steinberg, G. A dynein loading zone for retrograde endosome motility at microtubule plus-ends. *The EMBO journal* **25**, 2275-2286 (2006).
21. Markus, S.M. *et al.* Quantitative analysis of Pac1/LIS1-mediated dynein targeting: Implications for regulation of dynein activity in budding yeast. *Cytoskeleton* **68**, 157-174 (2011).
22. Elshenawy, M.M. *et al.* Lis1 activates dynein motility by modulating its pairing with dynactin. *Nature cell biology* **22**, 570-578 (2020).
23. Htet, Z.M. *et al.* LIS1 promotes the formation of activated cytoplasmic dynein-1 complexes. *Nature cell biology* **22**, 518-525 (2020).
24. Marzo, M.G., Griswold, J.M. & Markus, S.M. Pac1/LIS1 stabilizes an uninhibited conformation of dynein to coordinate its localization and activity. *Nature cell biology* **22**, 559-569 (2020).

25. Qiu, R., Zhang, J. & Xiang, X. LIS1 regulates cargo-adapter-mediated activation of dynein by overcoming its autoinhibition in vivo. *J Cell Biol* (2019).
26. Markus, S.M. & Lee, W.L. Regulated offloading of cytoplasmic dynein from microtubule plus ends to the cortex. *Developmental cell* **20**, 639-651 (2011).
27. Toropova, K. *et al.* Lis1 regulates dynein by sterically blocking its mechanochemical cycle. *eLife* **3** (2014).
28. Yamada, M. *et al.* LIS1 and NDEL1 coordinate the plus-end-directed transport of cytoplasmic dynein. *The EMBO journal* **27**, 2471-2483 (2008).
29. Torisawa, T. *et al.* Functional dissection of LIS1 and NDEL1 towards understanding the molecular mechanisms of cytoplasmic dynein regulation. *The Journal of biological chemistry* **286**, 1959-1965 (2011).
30. Reck-Peterson, S.L. *et al.* Single-molecule analysis of dynein processivity and stepping behavior. *Cell* **126**, 335-348 (2006).
31. DeWitt, M.A., Chang, A.Y., Combs, P.A. & Yildiz, A. Cytoplasmic dynein moves through uncoordinated stepping of the AAA+ ring domains. *Science* **335**, 221-225 (2012).
32. Qiu, W. *et al.* Dynein achieves processive motion using both stochastic and coordinated stepping. *Nature structural & molecular biology* **19**, 193-200 (2012).
33. Belyy, V., Hendel, N.L., Chien, A. & Yildiz, A. Cytoplasmic dynein transports cargos via load-sharing between the heads. *Nature communications* **5**, 5544 (2014).
34. Belyy, V. *et al.* The mammalian dynein-dynactin complex is a strong opponent to kinesin in a tug-of-war competition. *Nature cell biology* **18**, 1018-1024 (2016).
35. Elshenawy, M.M. *et al.* Cargo adaptors regulate stepping and force generation of mammalian dynein-dynactin. *Nat Chem Biol* **15**, 1093-1101 (2019).
36. Gutierrez, P.A., Ackermann, B.E., Vershinin, M. & McKenney, R.J. Differential effects of the dynein-regulatory factor Lissencephaly-1 on processive dynein-dynactin motility. *The Journal of biological chemistry* **292**, 12245-12255 (2017).
37. Ferro, L.S. *et al.* Structural and functional insight into regulation of kinesin-1 by microtubule-associated protein MAP7. *Science* **375**, 326-331 (2022).
38. Gennerich, A., Carter, A.P., Reck-Peterson, S.L. & Vale, R.D. Force-induced bidirectional stepping of cytoplasmic dynein. *Cell* **131**, 952-965 (2007).
39. Nicholas, M.P. *et al.* Cytoplasmic dynein regulates its attachment to microtubules via nucleotide state-switched mechanosensing at multiple AAA domains. *Proceedings of the National Academy of Sciences of the United States of America* **112**, 6371-6376 (2015).
40. Rao, L., Berger, F., Nicholas, M.P. & Gennerich, A. Molecular mechanism of cytoplasmic dynein tension sensing. *Nature communications* **10**, 3332 (2019).
41. Ezber, Y., Belyy, V., Can, S. & Yildiz, A. Dynein harnesses active fluctuations of microtubules for faster movement. *Nature Physics* **16**, 312-316 (2020).
42. McKenney, R.J., Vershinin, M., Kunwar, A., Vallee, R.B. & Gross, S.P. LIS1 and NudE induce a persistent dynein force-producing state. *Cell* **141**, 304-314 (2010).
43. Kon, T., Mogami, T., Ohkura, R., Nishiura, M. & Sutoh, K. ATP hydrolysis cycle-dependent tail motions in cytoplasmic dynein. *Nature structural & molecular biology* **12**, 513-519 (2005).
44. Cleary, F.B. *et al.* Tension on the linker gates the ATP-dependent release of dynein from microtubules. *Nature communications* **5**, 4587 (2014).
45. Jha, R., Roostalu, J., Cade, N.I., Trokter, M. & Surrey, T. Combinatorial regulation of the balance between dynein microtubule end accumulation and initiation of directed motility. *The EMBO journal* **36**, 3387-3404 (2017).
46. Baumbach, J. *et al.* Lissencephaly-1 is a context-dependent regulator of the human dynein complex. *eLife* **6** (2017).

47. Lammers, L.G. & Markus, S.M. The dynein cortical anchor Num1 activates dynein motility by relieving Pac1/LIS1-mediated inhibition. *J Cell Biol* **211**, 309-322 (2015).

Methods

Protein purification and labeling

The endogenous genomic copies of *S. cerevisiae* dynein heavy chain (*DYN1*) and Lis1 (*PAC1*) were modified or deleted using homologous recombination[30]. The list of strains used in this study is shown in Extended Data Table 1. *S. cerevisiae* strains that express dynein, $dynein_{Gal}$, and Lis1 constructs were grown in 2 L YPA-galactose media (1% yeast extract, 1% peptone, % 0.004 adenine sulfate, 2% galactose) until OD_{600} reaches 2.0. The cells were pelleted at 6,000 *g* for 15 min, resuspended in phosphate buffer saline (PBS), and frozen in liquid nitrogen. For purification of dynein and $dynein_{Gal}$, cell pellets were grinded and then dissolved in the lysis buffer (30 mM HEPES pH 7.4, 50 mM KAc, 2 mM $Mg(Ac)_2$, 1 mM EGTA, 10% glycerol, 1 mM DTT, 0.1 mM ATP, 1 mM phenylmethylsulfonyl fluoride (PMSF), 0.1% Triton) at 37°C. The lysate was centrifuged at 500,000 *g* for 45 min and the supernatant was incubated with 300 µL IgG beads for 1 h at 4 °C. The mixture was then applied to Qiagen columns, washed with 30 mL lysis buffer supplemented with 250 mM KAc, and then with 20 mL TEV buffer (10 mM Tris-HCl pH 8.0, 150 mM KCl, 10% glycerol, 1 mM DTT, 0.1 mM ATP, 0.25 mM PMSF) at 4 °C. The mixture was then incubated with 10 µL 2 mg mL^{-1} TEV protease for 1 h at 4 °C. The eluted protein was separated from the beads by centrifuging the mixture in Amicon Ultra Free MC tubes at 21,000 *g* for 2 min, flash-frozen in liquid nitrogen, and stored at -80 °C. A similar procedure was used to purify Lis1, except cells were lysed in a hi-salt phosphate lysis buffer (50 mM potassium phosphate pH = 8.0, 150 mM KAc, 2 mM $Mg(Ac)_2$, 10% glycerol, 10 mM Imidazole, 150 mM NaCl, 50 mM 2-Mercaptoethanol (BME), 1 mM PMSF, 0.2% Triton) and protein was eluted in nu-TEV buffer (50 mM Tris-HCl pH 8.0, 1 mM EGTA, 150 mM KAc, 150 mM NaCl, 2 mM $Mg(Ac)_2$, 10% glycerol, 1 mM DTT, 0.5 mM PMSF). The protein concentration was determined by both 280 nm absorbance and the Bradford assay.

Proteins were labeled with fluorescent dyes after resuspending the lysate with beads and before adding TEV protease. 10 nanomoles of a fluorescent dye were well mixed with the protein-bead mixture and incubated for 1 h at 4 °C. The column was then washed with 100 mL TEV buffer to remove excess dye before eluting the protein from beads. The labeling percentage was determined by measuring the protein concentration in Bradford assays and the absorbance under 555 nm and 655 nm excitation for TMR/LD555 and Cy5/LD655 dyes, respectively. The probability, p of each SNAP-Lis1 monomer labeled with TMR and LD655 dyes derivatized with benzyl guanine was 72% and 80% per Lis1 monomer, respectively. The probabilities of a SNAP-Lis1 dimer to be labeled with at least one TMR or LD655 dyes (calculated as $2p - p^2$) were 92% and 96%, respectively.

Microtubule Polymerization and Subtilisin Treatment

Tubulin was purified from pig brains in 1 M PIPES buffer. 60 ng unlabeled tubulin, 60 ng biotinylated tubulin, and 1 ng fluorescently-labeled tubulin were diluted to 1 mg ml^{-1} in 120 µL BRB80 buffer (80 mM PIPES pH = 6.8, 2 mM $MgCl_2$, 1 mM EGTA) supplemented with 1x polymerization mixture (1mM GTP, 10% DMSO) and polymerized at 37 °C for 40 min and another 40 min after supplementing the mixture with 1 mM taxol. The mixture was centrifuged at 21,000 *g* for 13 min at room temperature and resuspended in 30 µL BRB80 buffer supplemented with 10 mM taxol and 1 mM DTT. Microtubules were stored in dark at room temperature and used within seven days.

For subtilisin treatment, polymerized microtubules were stored in dark for 1 day for elongation and then incubated with a 1:100 (w/w) subtilisin to tubulin ratio for 2 h at a 37 °C bath. The proteolytic cleavage was stopped with the addition of 2 mM PMSF. The microtubules were centrifuged at 21,000 *g* for 13 min at room temperature and the pellet was resuspended in BRB80 supplemented with 10 mM taxol.

Single-molecule motility assays

Flow channels were prepared by placing a multichannel parafilm in between a microscope slide and a cover glass functionalized with PEG/PEG-biotin (Microsurfaces Inc.). The channel was incubated with 20 µL of 2 mg mL^{-1} streptavidin for 2 min and excess streptavidin was removed by washing the channel with 60 µl DP buffer (DLB with 10% glycerol, 2% pluronic acid, 1 mM taxol, 1 mM tris(2-carboxyethyl)phosphine (TCEP)). The channel was then incubated with 20 µl of 2 mg mL^{-1} biotinylated microtubules in DP buffer for 2 min and unbound microtubules were removed by washing the channel with 60 µl DP buffer and then with 20 µl DM buffer (DLB supplemented with 10% glycerol, 0.4% pluronic, 1 mM taxol, 1 mM TCEP). After 3 min, the channel was then washed with 20 µL of stepping buffer (93% DM buffer, 2 mM ATP, gloxy (glucose oxidase and catalase), 0.5% dextrose, and 50 -150 mM KAc). Dynein and Lis1 were diluted in stepping buffer and incubated on ice for 10 min. 20 µL motor+Lis1 final mixture in stepping buffer was added to the channel and the sample was imaged immediately for 15 min.

Lis1-dynein colocalization experiments were performed by mixing fluorescently-labeled dynein and Lis1 into the final mixture, before flowing into the chamber. Colocalization between two differentially labeled dynein was performed by mixing 5 nM LD555 dynein with LD655-dynein and letting on ice for 10 min with or without Lis1. To maximize crosslinking efficiency with different colors of dyneins, dyneins were added to the mixture before Lis1. Dynein-Lis1 mixture was diluted in stepping buffer supplemented with 1 mM ATP and 50 mM KAc.

Single-molecule imaging was performed using a custom-built objective-type TIRF microscope equipped with an inverted microscopy body (Nikon Ti-Eclipse), 100× magnification 1.49 numerical aperture (N.A.) plan-apochromat oil-immersion objective (Nikon), and a perfect focusing system. The fluorescence signal was detected using an electron-multiplied charge-coupled device (EM-CCD) camera (Andor, Ixon). The effective pixel size after magnification was 108 nm. Samples labeled with GFP, TMR/LD555, and Cy5/LD655 were excited using 0.04 kW cm^{-2} 488, 532, and 633 nm laser beams (Coherent), and the emission signal was detected using bandpass emission filters (Semrock). For two- and three-color fluorescence assays, imaging was performed using alternating excitation and the time-sharing mode. Single color movies were recorded at 1 Hz, whereas multi-color movies were recorded with 0.5 s per frame per color using the time-sharing mode. To introduce or remove Lis1 from the channel during imaging, two 0.5 mm diameter holes were drilled on a glass slide at both ends of the flow channel. The region of interest in the channel was imaged for 1 min before introducing Lis1 or washing the free Lis1 from the channel while imaging dynein motility in real-time.

Data Analysis

Movies were analyzed in ImageJ to create kymographs. Motors that are stationary, exhibit diffusional movement, or move less than 3 pixels were excluded from the analysis. The results of the data analysis were plotted in Prism and Origin. Data fitting was performed in Origin. Cumulative distribution functions

(CDFs) of the run length and run-time data were fitted to a double exponential decay, $y = A_1 e^{-t/\tau_1} + A_2 e^{-t/\tau_2}$ where A_1 and A_2 are the amplitudes and τ_1 and τ_2 are the decay constants. The weighted average of the decay constants, $\tau_{av} = \frac{A_1\tau_1 + A_2\tau_2}{A_1 + A_2}$ was reported as the decay constant.

The average velocities of motors that colocalize with 0 (V_0), 1 (V_1), and 2 (V_2) colors of Lis1 were determined from two- and three-color TIRF assays. To determine K_D of Lis1, the average dynein velocity under different Lis1 concentrations, V ($[Lis1]$) was fitted to $(1-p_b)^2 V_0 + 2p_b(1-p_b)V_1 + (p_b)^2 V_2$ where $p_b = \frac{1}{1+\frac{K_D}{[Lis1]}}$ is the binding probability of Lis1 to a dynein monomer. The probability of Lis1 colocalization to $\text{dynein}_{\text{Gal}}$ in Extended Data Figure 4c was fitted to a binding isotherm function, defined as $C(2p_b - (p_b)^2)$, where C is less than 1 due to incomplete labeling of Lis1 and the limited single-molecule detection ability due to the presence of excess labeled Lis1 in solution.

Microtubule co-pelleting assays

Unlabeled taxol-stabilized microtubules were polymerized as above and free tubulin was removed by centrifugation through a 60% glycerol gradient in BRB80 (80 mM PIPES-KOH pH 6.8, 1 mM magnesium chloride, 1 mM EGTA, 1 mM DTT, 20 µM Taxol) for 15min at 100,000xg and 37 °C. The microtubule pellet was resuspended in DLB supplemented with 20 µM taxol. Microtubules (0-600nM tubulin) were incubated with 100 nM Lis1 for 10 min before being pelleted for 15 min at 100,000xg and 25 °C. The supernatant was analyzed via SDS-PAGE and depletion was determined using densitometry in ImageJ. Binding curves were fit in Prism8 (GraphPad) with a nonlinear regression for one site binding with B_{max} set to 1.

Optical trapping assays

Optical trapping experiments were performed on a custom-built optical trap using a Nikon Ti-E microscope body and a 100× 1.49 NA plan-apochromat oil immersion objective, as previously described[33]. The beads were trapped with a 2W 1,064 nm laser (IPG Photonics) and the trap was steered with a two-axis acousto-optical deflector (AA Electronics). The trap stiffness was calculated from the Lorentzian fit to the power spectrum of a trapped bead. For stall force measurements, the trap stiffness was adjusted to allow the motor to walk 100 nm away from the trap center before the bead comes to stall. The position of the bead from the center of the fixed trap was recorded for at least 90 s at 5 kHz.

For fixed trap measurements, 0.8 µm diameter carboxylated latex beads (Life Technologies) were functionalized with rabbit polyclonal GFP antibody (BioLegend, no. MMS-118P), as previously described[33]. The 2 µL of the bead stock were diluted in 8 µL DLB. 2 µL of diluted beads were sonicated for 8 s. To ensure that more than 90% of the beads are driven by single motors, GFP-dynein concentration was diluted in the stepping buffer (93% DLBM buffer (DLB supplemented with 10% glycerol, 0.25 mM casein, 1 mM taxol, 1 mM TCEP), 2 mM ATP, 1% gloxy, 0.5% dextrose, and 50 mM KAc) to desired concentrations such that less than 30% of the beads exhibit motility when brought on top of a surface-immobilized axoneme. The mixture was sonicated for 8 s and 2 µL of diluted beads were mixed with 2 µL of GFP-dynein, 1.5 µL Lis1, and 2 µL stepping buffer, and incubated on ice for 10 min. For the no Lis1 condition, an equal volume of stepping buffer was added to the mixture instead of Lis1.

Cy5-labeled sea urchin axonemes were nonspecifically adsorbed to the channel surface. After 30 s, the channel was washed with 60 µL DLBC buffer (DLB with 10% glycerol, 2 mM casein, 1 mM taxol, and 1 mM TCEP) to remove the unbound axoneme. After 3 min, the channel was washed with 60 µL DLBM buffer and then with 20 µL stepping buffer. 7.5 µL of the dynein-Lis1-bead mixture was diluted in 20 µL stepping buffer and the KAc concentration was adjusted to 50 mM before being flown into the channel. The channel was sealed with nail polish to prevent evaporation during data acquisition.

Optical trap data were analyzed with a custom-written MATLAB script. The data were downsampled to 500 Hz via median filtering before analysis. Stall events were manually scored when the velocity of the bead movement was reduced to ~0 nm s^{-1} under hindering load and terminated with a sudden (<4 ms) snapping of the bead to the trap center. Events that occur within 25 nm distance to the trap center, last shorter than 0.4 s, or terminate with backward movement, multiple-step detachment, or slow (>4 ms) return of the bead to the trap center were excluded from the analysis. Stall forces were calculated as the average force value of the plateau where the bead is nearly immobile before detaching from the axoneme. Stall time was defined as the time the bead spends at the 30% margin of the stall force before it detaches from an axoneme. CDFs of stall times were fitted to a double exponential decay and the weighted average of two decay constants from the fit was reported as the decay constant.

F-V measurements

Similar sample preparation procedures were used for F-V measurements using an optical trap. After the bead movement reached half of the measured stall force of the motor, the trapping beam repositioned itself and maintained a 100 nm distance from the bead via a force-feedback mechanism. To determine the microtubule polarity in the no-ATP condition, unlabeled axonemes were immobilized to the channel and LD655-labeled GST-Dyn_{331kDA} motors (without a GFP tag) were flown into the channel in a stepping buffer supplemented with 30 µM ATP. The motors were allowed to walk on and accumulate at the minus-end of surface-immobilized axonemes for 4 mins. The channel was then washed with 40 µl with DLBM buffer, followed by 20 µl stepping buffer supplemented with 0.5 U ml^{-1} apyrase instead of ATP to deplete residual ATP in the channel. 0.5 U ml^{-1} apyrase was also included in the bead-dynein-Lis1 mixture to remove residual ATP from protein preparations. During optical trapping, microtubule polarity was determined by the minus-end accumulation of the LD655 signal determined by an sCMOS camera (Hamamatsu, Orca Flash 4.0). Beads were pulled along the length of an axoneme at a constant velocity, and the beads that engaged with the axoneme were trapped by repositioning the trapping beam 100 nm away from the bead center along the direction of the applied force.

The bead position was recorded at 5 kHz and the data were downsampled to 500 Hz via median filtering. The slope of each trace was defined as the velocity of individual motors under an applied force. The traces that are shorter than 70 ms, show bidirectional motility under load, or exhibit instantaneous jumps larger than 50 nm were excluded from data analysis. The asymmetry ratios were calculated by comparing the average velocities under forces equally larger or smaller than F_{stall}. Velocities at corresponding forces were either directly measured or calculated by linear regression of the measured velocities under the closest force measurements. The errors of asymmetry ratios were determined by error propagation of the compared velocities.

Statistical Analysis The p-values were calculated by the two-tailed t-test for stall force histograms, the two-tailed t-test with Welch corrections for velocity measurements, and the Kolmogorov-Smirnov test for run length and run time measurements in Prism and Origin. CDFs were calculated in MATLAB.

Figures

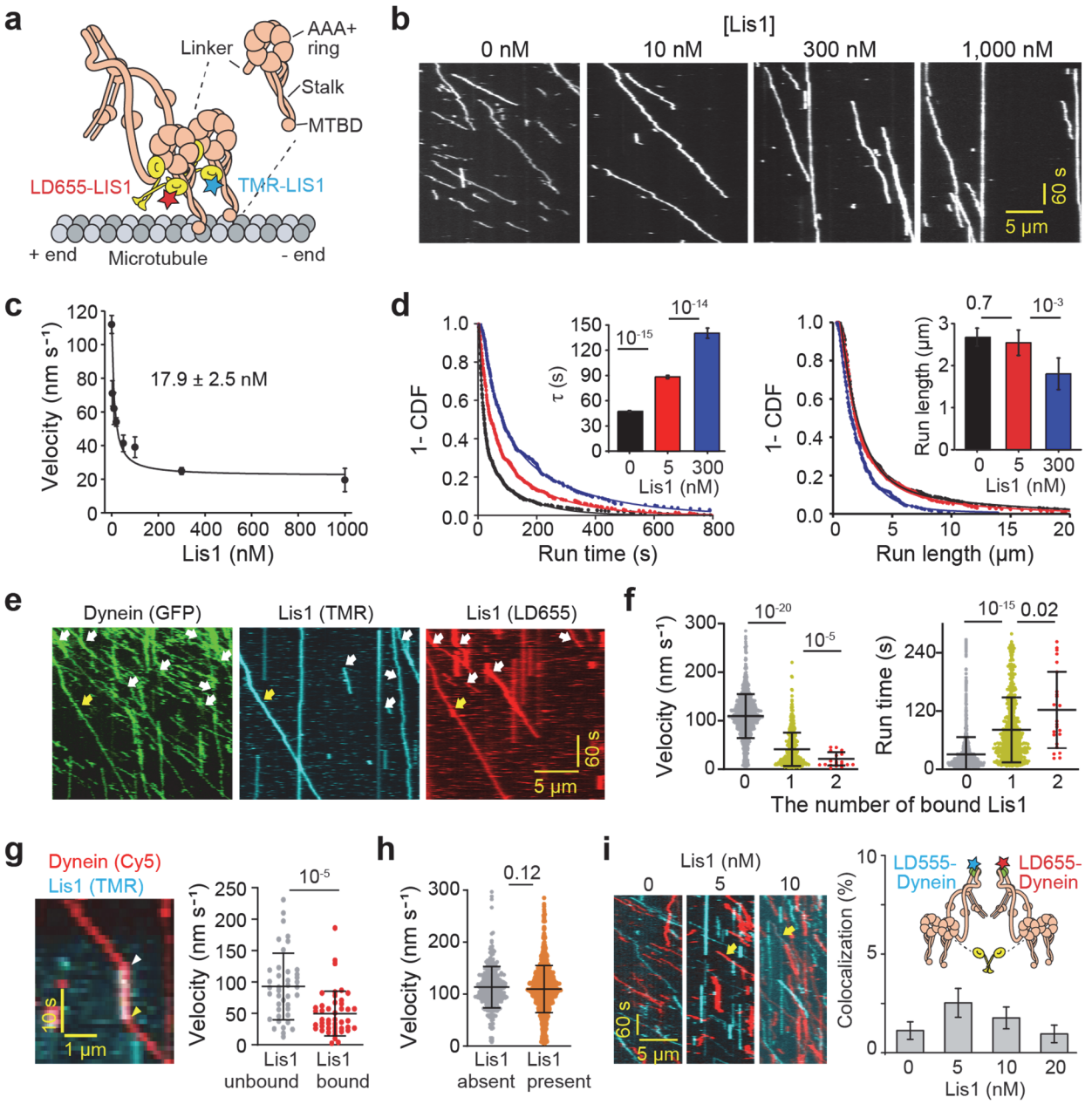

Figure 1 | Lis1 binding reduces the velocity while increasing the microtubule residence time of dynein. **a**) Schematic of the single-molecule motility of yeast cytoplasmic dynein in the presence of fluorescently-labeled Lis1. **b)** Representative kymographs of dynein with increasing concentrations of unlabeled Lis1. **c)** The velocity of dynein under different Lis1 concentrations in 50 mM KAc, respectively (mean ± s.e.m.; N = 861, 534, 233, 352, 278, 312, 131 for 0, 5, 10, 20, 50, 100, 300, and 1,000 nM Lis1; three biological replicates). The fit of the velocity data (solid curve) reveals K_D (±s.e., see Methods). **d)** The inverse cumulative distribution function (1-CDF) of run time and run length under different Lis1 concentrations. Fits to a double exponential decay (solid curves) reveal average run time and run length in each condition (bar graphs, ± s.e.; N = 861, 534, 312 from left to right). **e)** A representative kymograph of GFP-dynein in

the presence of 2 nM LD655- and 2 nM TMR-labeled Lis1. Arrows highlight processive motors colocalized with single (white) and two (yellow) colors of Lis1. **f)** The velocity and run time of dynein motors colocalized with 0, 1, and 2 Lis1s (mean ± s.d., N = 1706, 671, and 24 from left to right). **g)** (Left) A representative trace of transient binding (white arrowhead) and unbinding (yellow arrowhead) of Lis1 from processively walking dynein. (Right) The velocity of Lis1 unbound and bound sections of individual dynein trajectories (mean ± s.d., N = 41 and 45). **h)** The velocity distribution in the absence of Lis1 compared to the motors that do not colocalize with Lis1 when fluorescently-labeled Lis1 is present in the chamber (N = 361 and 1534, from left to right). **i)** (Insert) Schematic shows whether a single Lis1 dimer can crossbridge two dynein dimers labeled with different dyes. (Left) Example kymographs 5 nM LD555-dynein (cyan) and 5 nM LD655-dynein (red) in the presence of different Lis1 concentrations. Yellow arrows show colocalization between LD555 and LD655 dyes. (Right) The percentage of dynein trajectories that exhibit colocalization between LD555 and LD655 dyes (N = 408, 378, 426, and 208 from left to right, three independent experiments). In **f**, **g**, and **h**, the centerline and whiskers represent the mean and s.d., respectively. In **d**, **f**, **g**, and **h**, P-values were calculated by a two-tailed t-test with Welch correction for velocity and by Kolmogorov-Smirnov test for run time and run length.

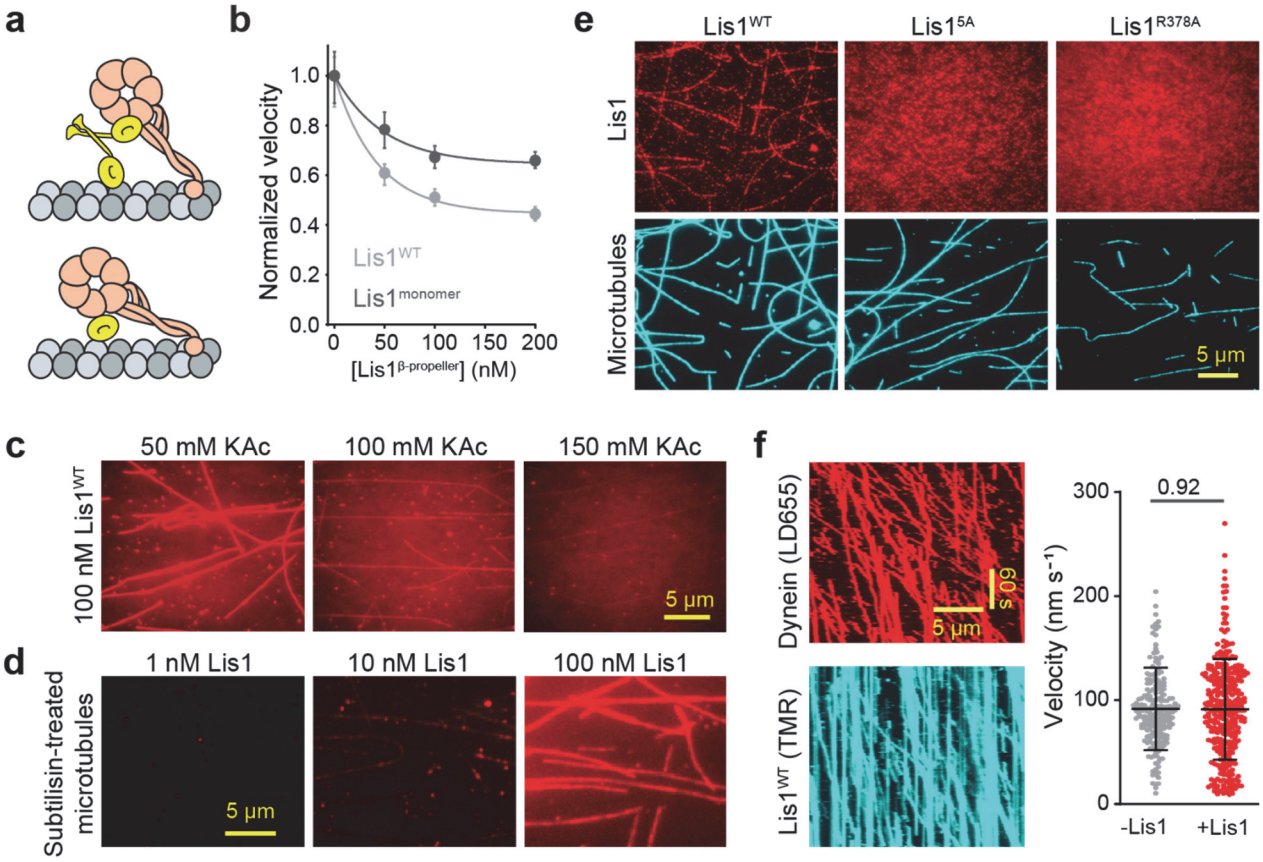

Figure 2 | Lis1's interaction with microtubules does not slow down dynein motility. a) Models of dynein tethered to a microtubule via a Lis1 dimer with one Lis1 ß-propeller docked to dynein and the other on the microtubule (top) or one Lis1 ß-propeller simultaneously interacts with dynein and the microtubule (bottom). **b)** Single-molecule velocity of dynein with increasing concentrations of $Lis1^{WT}$ or $Lis1^{monomer}$. The median and interquartile ranges are shown. Data were normalized to a velocity in the absence of Lis1. At least 400 single molecule events were measured per condition. **c)** Lis1 binding to surface-immobilized microtubules under different salt concentrations. **d)** Lis1 decorates subtilisin-treated microtubules in the presence of 50 mM KAc. **e**) Two-color imaging of Cy3-labeled microtubules and LD655-labeled $Lis1^{WT}$, $Lis1^{5A}$, or $Lis1^{R378A}$. Lis1 concentration was set to 100 nM and the assays were performed in a buffer containing 50 mM KAc. **f)** (Left) A representative kymograph of dynein motility on Lis1-decorated microtubules. Runs in the Lis1 channel colocalize with dynein. (Right) Velocities of dynein motors on undecorated (-Lis1) and Lis1-decorated (+Lis1) microtubules. (N= 208 and 329, from left to right). The center line and whiskers represent the mean and s.d., respectively. The P-value was calculated by a two-tailed t-test with Welch correction.

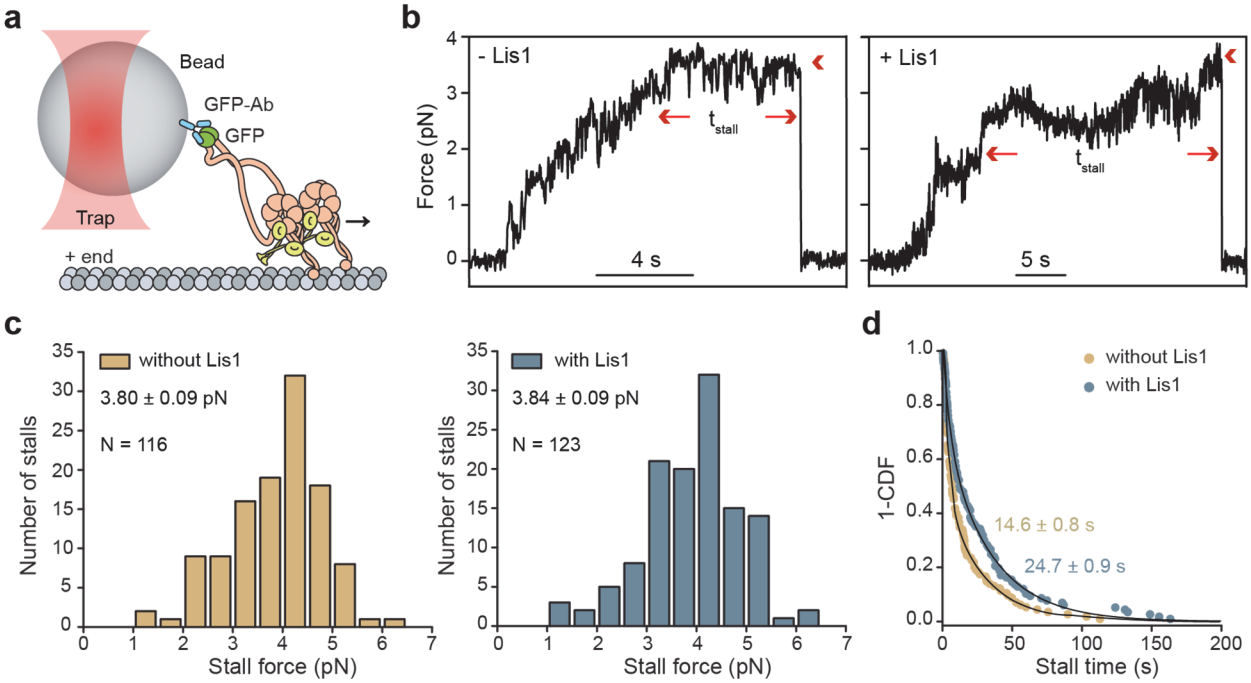

Figure 3 | Lis1 does not affect the stall force of dynein. a) The schematic shows stall force measurements of GFP-dynein in the presence of unlabeled Lis1 using a fixed-beam optical trap. **b)** Sample trajectories of beads driven by single dynein motors with and without 300 nM Lis1. The arrows show the beginning and the end of a stalling event (t_{stall}: stall duration). The arrowheads indicate the detachment of the motor from the microtubule and the snapping of the bead to the trap center. **c)** The stall force histogram of dynein in the presence and absence of 300 nM Lis1 (mean ±s.e.m.; $p = 0.77$, two-tailed t-test). **d)** Stall durations of dynein with and without 300 nM Lis1. Fit to a double exponential decay (solid curves) reveals the average stall duration (±s.e.).

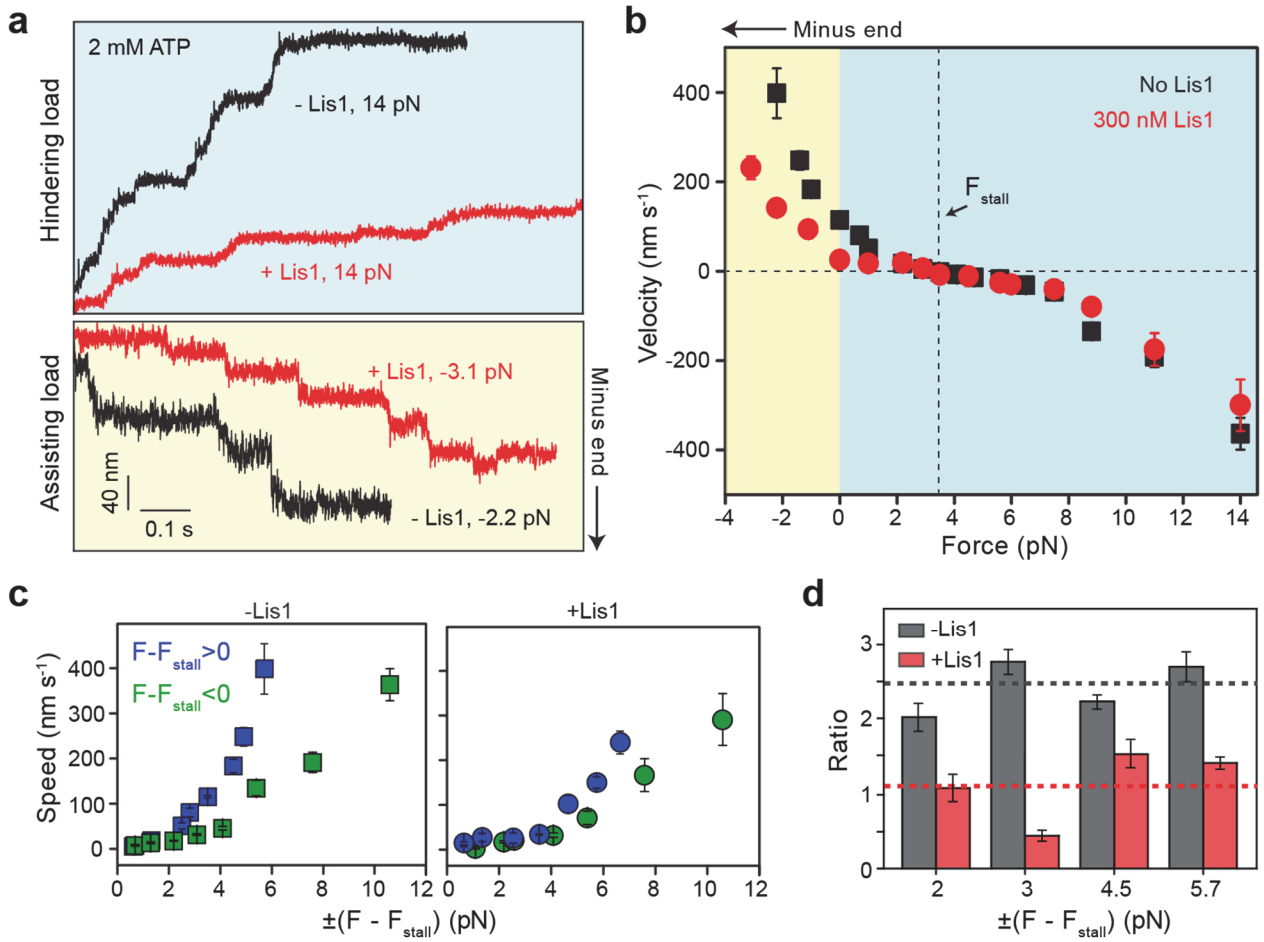

Figure 4 | Lis1 reduces the asymmetry in the F-V behavior of dynein. a) Representative traces of dynein-driven beads under assisting and hindering loads with and without 300 nM Lis1. Assays were performed in 1 mM ATP and 50 mM KAc. **b)** F-V measurements of dynein in the presence and absence of 300 nM Lis1 (mean ±s.e.m., from left to right, N = 41, 38, 37, 861, 27, 52, 106, 28, 51, 60, 89, 115, 124, 62, 23, 38, 40 without Lis1 and 34, 52, 25, 312, 33, 42, 49, 37 62, 47 33 42, 36, 29, 18 with Lis1). **c)** The speed of dynein-driven beads (mean ± s.e.m.) under the same magnitude of forces (F) in assisting and hindering directions relative to the stall force (F_{stall}). **d)** The ratios of the dynein speeds under the same magnitude of forces in assisting and hindering directions relative to F_{stall}. The dashed lines represent the average of the asymmetry ratios measured under different forces. The error bars represent s.e.m.

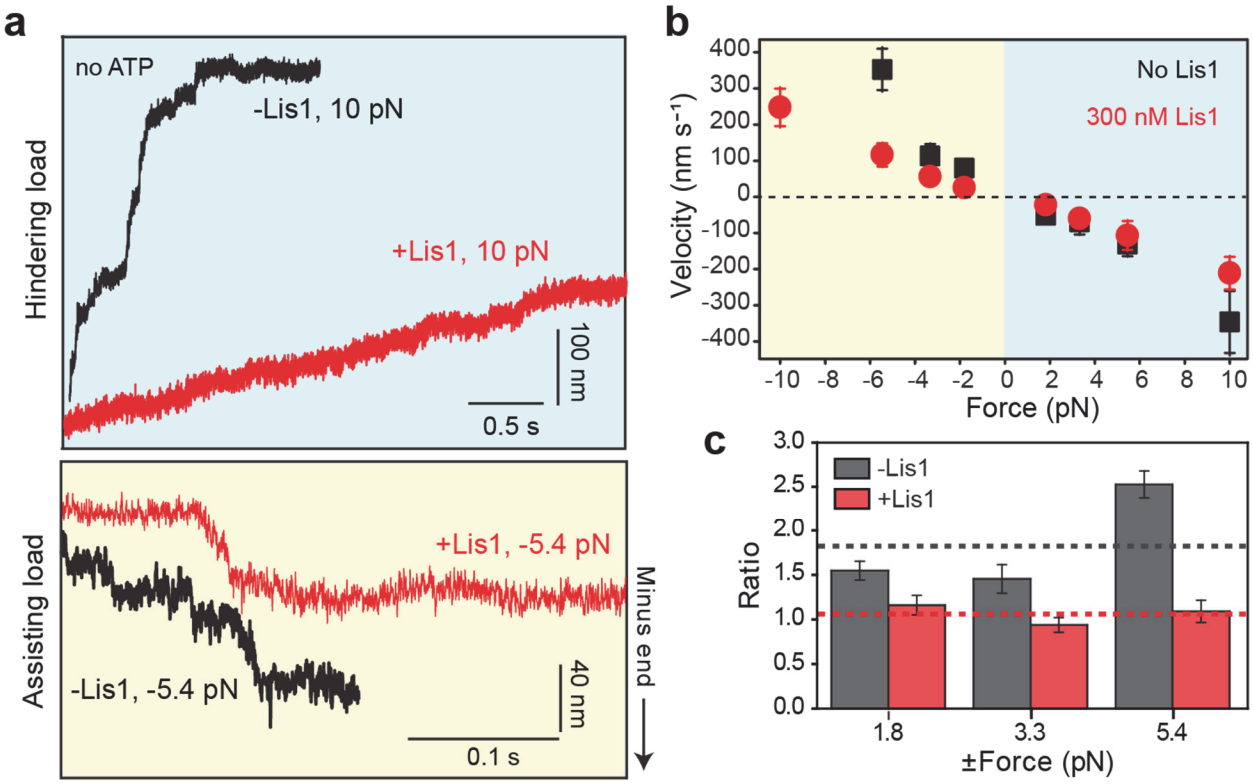

Figure 5 | Lis1-induced reduction of the asymmetry in the F-V behavior of dynein is independent of ATP. a) Representative traces of dynein-driven beads under assisting and hindering loads with and without 300 nM Lis1. Assays were performed in 50 mM KAc and without ATP. **b)** F-V measurements of dynein in the absence and presence of 300 nM Lis1 (mean ± s.e.m.; N = 42, 29, 65, 51, 38, 62, 15 without Lis1 and 36, 35, 34, 28, 21, 25, 20, 19 with Lis1 from left to right). **c)** The ratios of the velocities under the same magnitude of forces in assisting and hindering directions. The dashed lines represent the average of the asymmetry ratios measured under different forces. The error bars represent s.e.m.

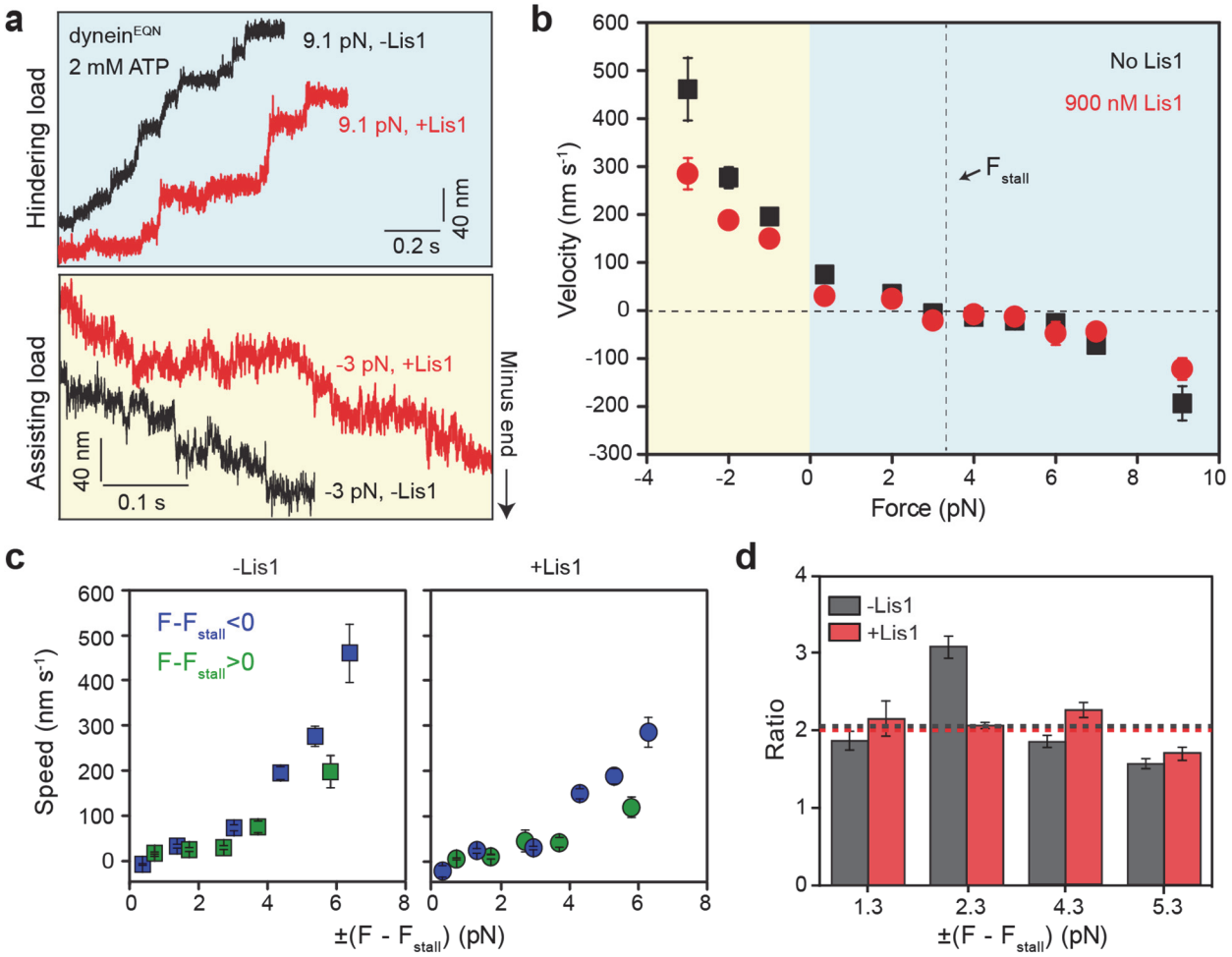

Figure 6 | Mutagenesis of the Lis1 binding site on the stalk recovers the asymmetry in the F-V behavior of dynein. a) Representative traces of dynein^{EQN}-driven beads under assisting and hindering loads with and without 900 nM Lis1. Assays were performed in 1 mM ATP and 50 mM KAc. **b)** F-V measurements of dynein^{EQN} with and without 900 nM Lis1 (mean ± s.e.m.; from left to right N = 31, 66, 62, 48, 47, 26, 42, 39, 23, 45, 33 without Lis1 and 54, 36, 61, 31, 37, 17, 54, 14, 19, 38, 26 with Lis1). **c)** The speed of dynein^{EQN}-driven beads (mean ± s.e.m.) under the same magnitude of forces in assisting and hindering directions relative to the dynein^{EQN} stall force (3.3 pN). **d)** The ratios of the velocities under the same magnitude of forces in assisting and hindering directions relative to the stall force. The dashed lines represent the average of the asymmetry ratios measured under different forces. The error bars represent s.e.m.

Extended Data

Strain	Construct	Genotype	Ref	Figures
RPY1732	GFP-dynein-DHA	MATa; *his3-11,15*; *ura3-1*; *leu2-3,112*; *ade2-1*; *trp1-1*; *pep4*Δ*::HIS5*; prb1Δ; ZZ-Tev-GFP-3XHA-*DYN1*-gs-DHA-Kan^{R}; nip100Δ; ndl1Δ::cgLEU2; pac1Δ::Hygro^{R}	This work	Fig. 1e-i, 2a,b,f, 3a-d, 4a-d, 5a-c, ED1a,b,ED2c,d, ED6a, ED9
RPY1736	GFP-dynein^{EQN}-DHA	MATa; *his3-11,15*; *ura3-1*; *leu2-3,112*; *ade2-1*; *trp1-1*; *pep4*Δ*::HIS5*; prb1Δ; ZZ-TEV-GFP-3XHA-*DYN1(E3012A, Q3014A, N3018A)*-gs-DHA-Kan^{R}; nip100Δ; ndl1Δ::cgLEU2; pac1Δ::Hygro^{R}	This work	Fig. 6a-d, ED8a-g, ED9
SM2344	HALO-dynein$_{gal}$	MATa; *nip100*Δ::*LEU2; ura3-1*::GAL1p-*DYN2*:GAL1p-*DYN3*:GAL1p-*PAC11*:GAL1p-8xHis-ZZ-2XTEV-HALO-*DYN1*::*URA3; his3-11,15*; *ura3-1; leu2-3,112*; *ade2-1*; *trp-1; pep4*Δ::*HIS5*; prb1Δ	24	ED2e,f, ED3a-c, ED4a-d, ED5a-d, ED6b,c
RPY1167	GFP-GST-Dyn$_{331kDa}$-DHA	MATa; *his3-11,15; ura3-1; leu2-3,112; ade2-1; trp1-1; pep4*Δ*::HIS5; prb1*Δ*;* P$_{GAL1}$-ZZ-Tev-GFP-3XHA-GST-*DYN1(331kDa)*-gs-DHA-Kan^{R}; *pac1*Δ*; ndl1*Δ*::cgLEU2*	15	ED7a-c
RPY228	GFP-GST-Dyn$_{314kDa}$-DHA	MATa; *his3-11,15; ura3-1; leu2-3,112*; *ade2-1; trp1-1*; *pep4*Δ::*HIS5; prb1*Δ; P$_{GAL1}$-ZZ-Tev-GFP-3xHA-GST-*DYN1(314kDa)*-gs-DHA	30	ED7a-c
RPY799	SNAP-Lis1	MATa*; his3-11,15; ura3-1; leu2-3,112; ade2-1; trp1-1; pep4*Δ*::HIS5; prb1*Δ*; dyn1*Δ*::cgLEU2;* P$_{GAL1}$-8HIS-ZZ-SNAP-gs-*PAC1*	15	Fig. 1e-h, 2c-f , ED1a,b, ED2h, ED4a-d, ED5a-d, ED6a-c, ED8c-d
RPY816	Lis1^{WT}	MATa*; his3-11,15; ura3-1; leu2-3,112; ade2-1; trp1-1; pep4*Δ*::HIS5; prb1*Δ*;* P$_{GAL1}$-8HIS-ZZ-Tev-*PAC1; dyn1*Δ*::cgLEU2; ndl1*Δ*::*Hygro^{R}	27	Fig. 1b-d,i, 3b-d, 4a-d, 5a-c, 6a-d, ED2c-g, ED3a-c, ED7a-c, ED8a,b,e-g, ED9
RPY1042	Lis1^{monomer}	MATa; *pep4D::HIS5; prb1D; GAL1-8HIS-ZZ-Tev-PAC1(aa 3-129 delete)-g-1XFLAG-gaSNAP-kanR; dyn1D::CgLEU2; ndl1D::HPH*	13	Fig 2b
RPY1544	Lis1^{R378A}	MATa*; his3-11,15; ura3-1; leu2-3,112; ade2-1; trp1-1; pep4*Δ*::HIS5; prb1*Δ*;* P$_{GAL1}$-8HIS-ZZ-Tev-*PAC1(R378A); dyn1*Δ*::cgLEU2; ndl1*Δ*::*Hygro^{R}	27	Fig. 2e
RPY1547	Lis1^{5A}	MATa*; his3-11,15; ura3-1; leu2-3,112; ade2-1; trp1-1; pep4*Δ*::HIS5; prb1*Δ*;* P$_{GAL1}$-8HIS-ZZ-Tev-*PAC1(R275A, R301A, R378A, W419A, K437A); dyn1*Δ*::cgLEU2; ndl1*Δ*::*Hygro^{R}	27	Fig. 2e, ED2b-g

Extended Data Table 1 | The list of *S. cerevisiae* strains used in this study. SNAP, DHA, and HALO are genetic tags used for labeling the protein with a fluorescent dye. Lis1 constructs that are not tagged with SNAP were labeled with maleimide reactive probes. TEV indicates a Tev protease cleavage site. P_{GAL1} denotes the galactose promoter, which was used for inducing strong expression of Lis1 and dynein motor domain constructs. Amino acid spacers are indicated by g (glycine) and gs (glycine-serine). (Ref: Reference, ED: Extended Data Figure).

Extended Data Figures

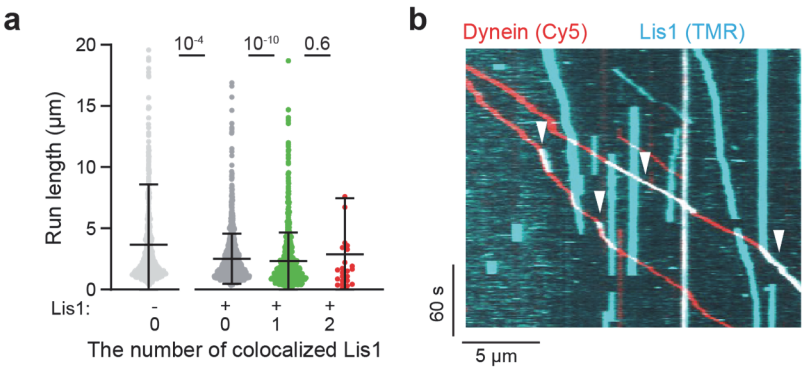

Extended Data Figure 1 | Transient binding of Lis1 slows down motility whereas Lis1 unbinding restores the velocity. a) The run length of dynein in the absence and presence of Lis1. In the presence of Lis1, run lengths were separately calculated for motors that colocalize with 0, 1, and 2 colors of Lis1. The center line and whiskers represent the mean and s.d., respectively. P-values were calculated by a Kolmogorov-Smirnov test. **b)** A representative kymograph shows that transient binding of Lis1 slows down whereas the subsequent release of Lis1 restores the velocity (arrowheads).

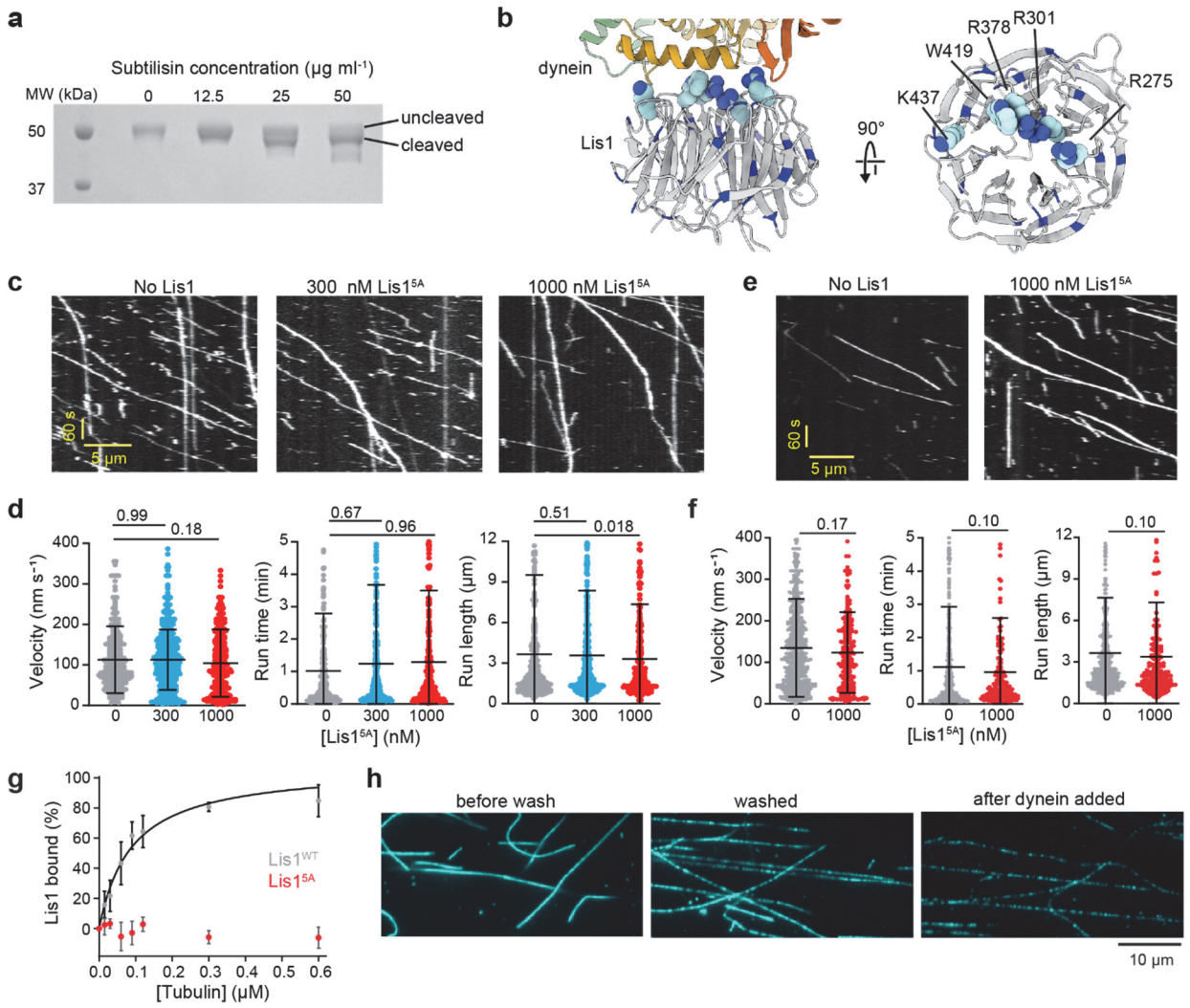

Extended Data Figure 2 | Lis1 interacts with the microtubule lattice through its dynein binding site in vitro. a) The subtilisin treatment of microtubules reduces the molecular weight of tubulin in a denaturing gel. **b)** The structure of Lis1 bound to the AAA ring with the five residues mutated in Lis1^{5A} are shown as spheres and all lysine and arginine residues are in blue. **c)** Representative kymographs of dynein in the presence and absence of Lis1^{5A}. **d)** The velocity, run time, and run length of dynein in the presence and absence of Lis1^{5A} (N = 326, 534, 336 from left to right). **e)** Representative kymographs of dynein$_{Gal}$ in the presence or absence of 1 μM unlabeled Lis1^{5A}. **f)** The velocity, run time, and run-length of dynein$_{Gal}$ in the presence or absence of 1 μM Lis1^{5A} (N = 610 and 209 from left to right). **g)** Microtubule co-pelleting assay with Lis1^{WT} and Lis1^{5A} (mean ±s.e.m., three replicates per condition). Statistical analysis was performed using an extra sum-of-squares F test; $p<0.0001$. **h)** Surface-immobilized microtubules were decorated by 100 nM TMR-Lis1 before and after removing unbound Lis1 in the channel. In **c-f**, assays were performed in 50 mM KAc. Assays in **h** were performed in the absence of added salt to maximize the Lis1-microtubule interaction. In **d** and **f**, the center line and whiskers represent the mean and s.d., respectively. P values were calculated by a two-tailed t-test with Welch correction for velocity and by Kolmogorov-Smirnov test for run time and run length.

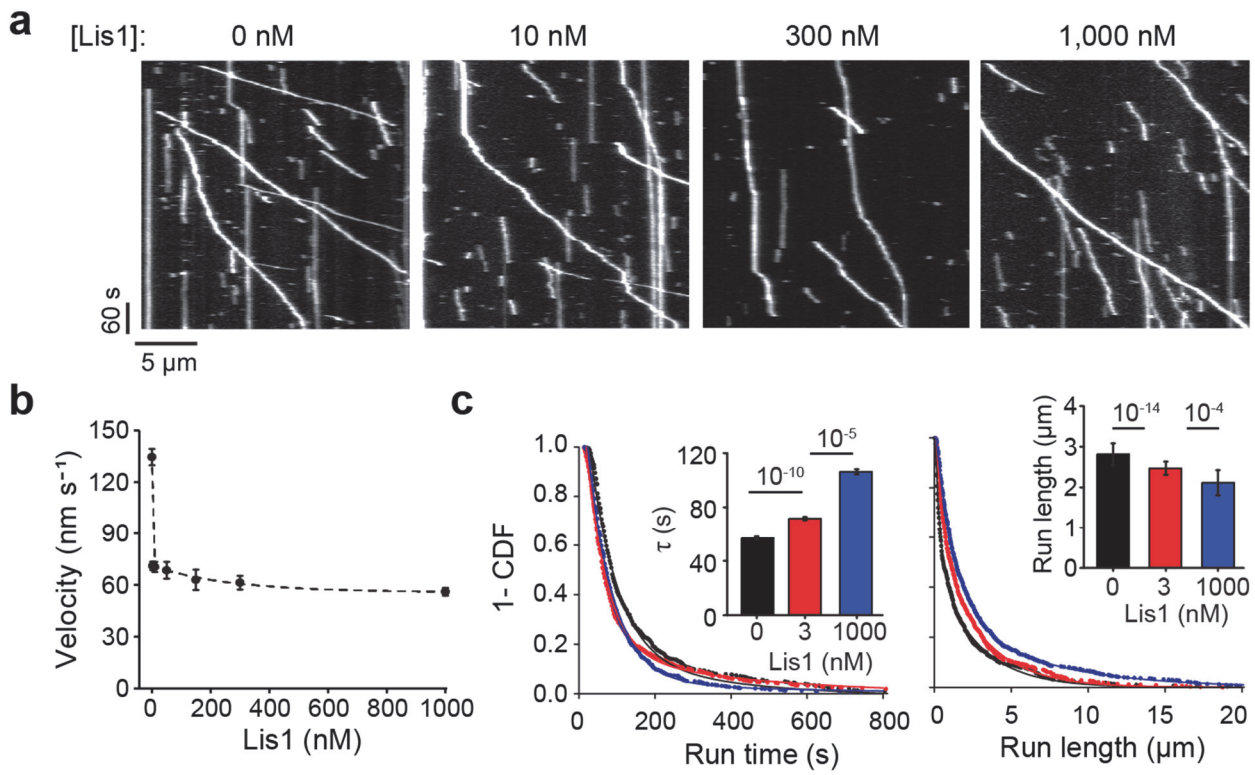

Extended Data Figure 3 | Motility of dynein$_{Gal}$ in the presence of unlabeled Lis1. a) Representative kymographs of dynein$_{Gal}$ with increasing concentrations of unlabeled Lis1. **b)** The velocity of dynein$_{Gal}$ under different Lis1 concentrations in 150 mM KAC (mean ± s.e.m.; N = 611, 694, 604, 230, 260, 251, 852 for 0, 3, 10, 50, 150, 300, and 1,000 nM Lis1, respectively; two biological replicates). **c)** The inverse cumulative distribution function of run time and run-length of dynein$_{Gal}$ under different Lis1 concentrations. Fits to a double exponential decay (solid curves) reveal the average run time and run length of the motor in each condition (bar graphs, ± s.e.; N = 611, 694, 251 from left to right).

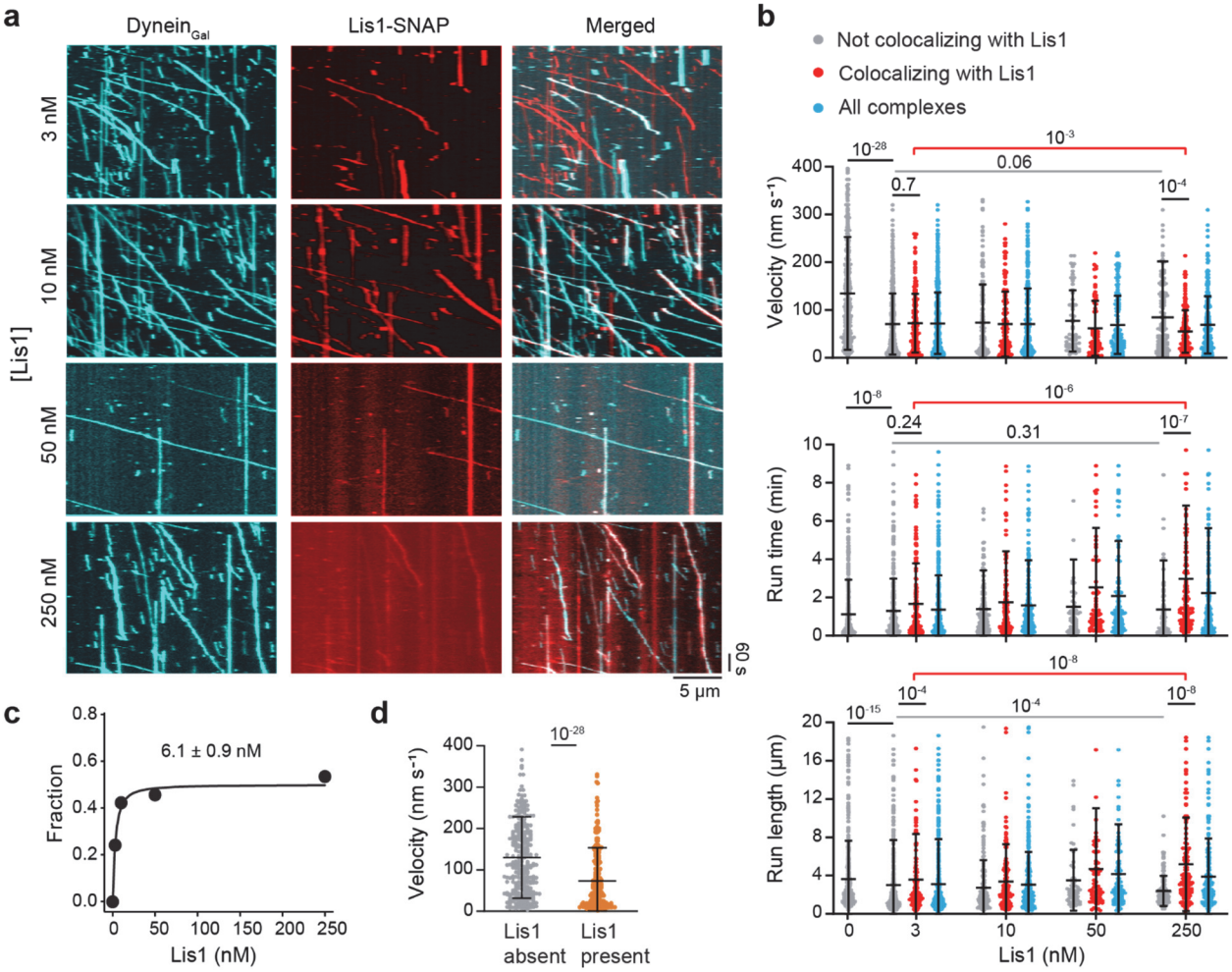

Extended Data Figure 4 | Motility of dynein$_{Gal}$ in the presence of fluorescently-labeled Lis1. a) Representative kymographs of two-color imaging of LD655-labeled dynein$_{Gal}$ and LD555-labeled Lis1 under different Lis1 concentrations. **b)** The velocity, run time, and run length distributions of dynein complexes under different concentrations of Lis1 (N = 611, 526, 168, 694, 233, 175, 408, 55, 69, 124,126, 145, 271 from left to right). **c)** The fraction of LD655-dynein complexes that colocalize with LD555-Lis1 under different Lis1 concentrations. A fit to a binding isotherm function (solid curve, see Methods) reveals K_D (±s.e.). **d)** The velocity distribution of dynein$_{Gal}$ in the absence of Lis1 compared to the motors that do not colocalize with Lis1 when fluorescently-labeled Lis1 is present in the chamber (N = 611 and 233 from left to right). In **b** and **d**, the centerline and whiskers represent the mean and s.d., respectively. P-values were calculated by a two-tailed t-test with Welch correction for velocity and by Kolmogorov-Smirnov test for run time and run length.

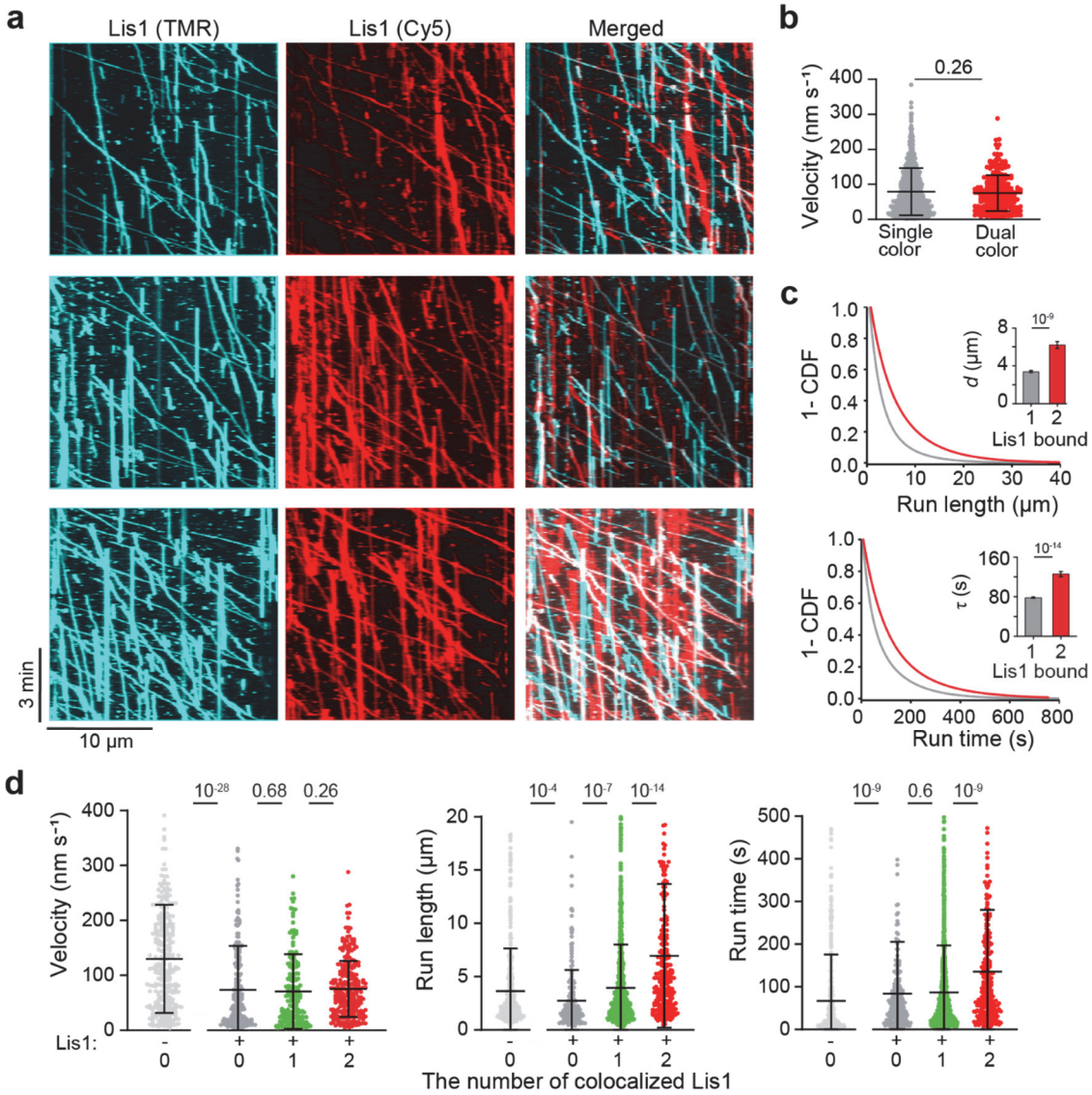

Extended Data Figure 5 | Binding of two Lis1s further increases the run time and run length, but not the velocity of dynein$_{Gal}$. a) Representative kymographs show colocalization of TMR- (5 nM) and Cy5-labeled (5 nM) Lis1 to unlabeled dynein$_{Gal}$. **b)** The velocity distribution of the trajectories that contain single (N = 811) or both (N = 216) colors of Lis1. The binding of second Lis1 to dynein$_{Gal}$ does not significantly reduce the velocity. **c)** Run length and run time of dynein$_{Gal}$ that colocalize with single (gray, N = 811) or both (red, N = 216) colors of Lis1. The binding of second Lis1 increases the run time and run length. Inserts show calculated run length and run time values (mean ± s.e.) from a fit to a double exponential decay (solid curves). P values were calculated by a Kolmogorov-Smirnov test. **d)** Velocity, run length, and run time distributions of dynein$_{Gal}$ in the absence and presence of Lis1 in the channel (N = 287, 233, 175, 274, from left to right). Dynein$_{Gal}$ motors that colocalize with 0, 1, or 2 colors of Lis1 were analyzed separately. In **b**, **c**, and **d**, the center line and whiskers represent the mean and s.d., respectively. P values were calculated by two-tailed t-tests with Welch correction for velocity and by Kolmogorov-Smirnov test for run time and run-length measurements.

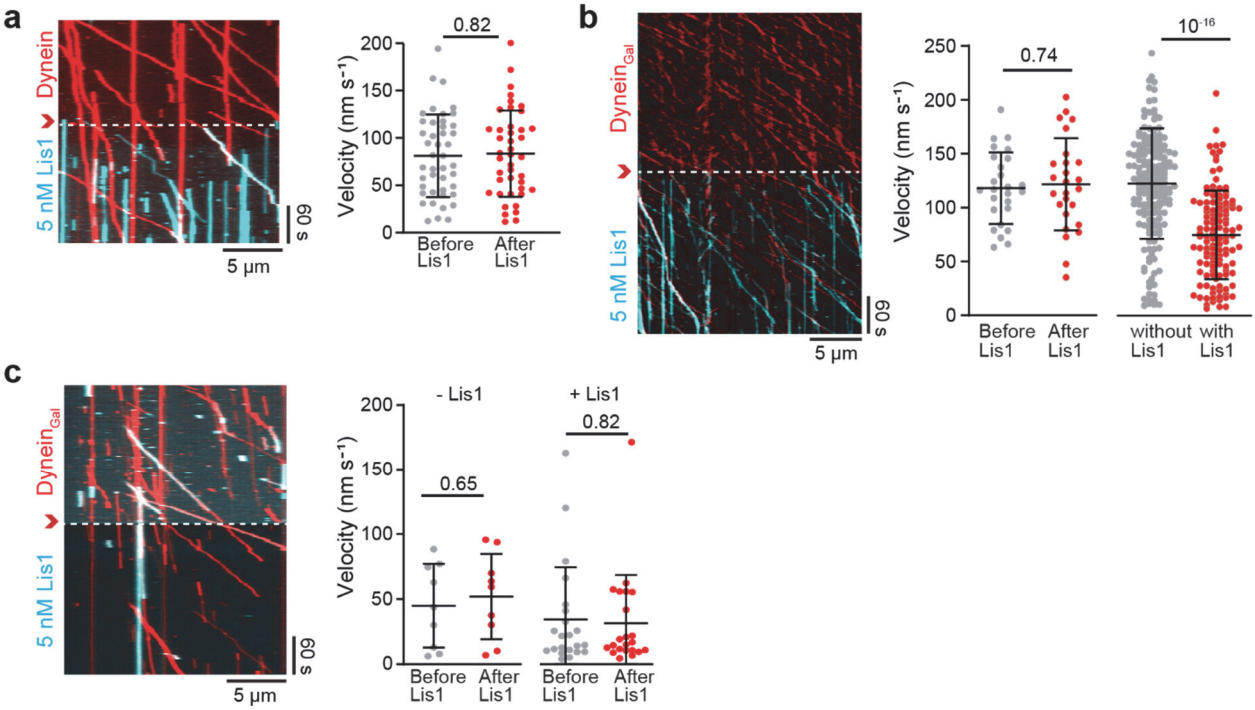

Extended Data Figure 6 | The addition and removal of Lis1 whilst recording dynein motility. a) A kymograph (left) and velocity (right) of dynein before and after Lis1 was flown into the flow chamber (N = 44 and 42 from left to right). **b)** A kymograph of dynein$_{Gal}$ when Lis1 was flown into the channel. (Middle) The velocity of the complexes that walk on the microtubules during Lis1 addition before and after flowing Lis1 (N = 26 and 26 from left to right). (Right) The velocity of the complexes that colocalize or do not colocalize with Lis1 after Lis1 addition (N = 122 and 84 from left to right). **c)** A kymograph (left) and velocity (right) of dynein$_{Gal}$ before and after washing excess Lis1 from the flow chamber. Complexes that colocalize (+Lis1) and not colocalize (-Lis1) with Lis1 were analyzed separately (N = 9, 9, 22, 22 from left to right). Assays were performed in 50 mM KAc. The center line and whiskers represent the mean and s.d., respectively. P-values were calculated by a two-tailed t-test with Welch correction.

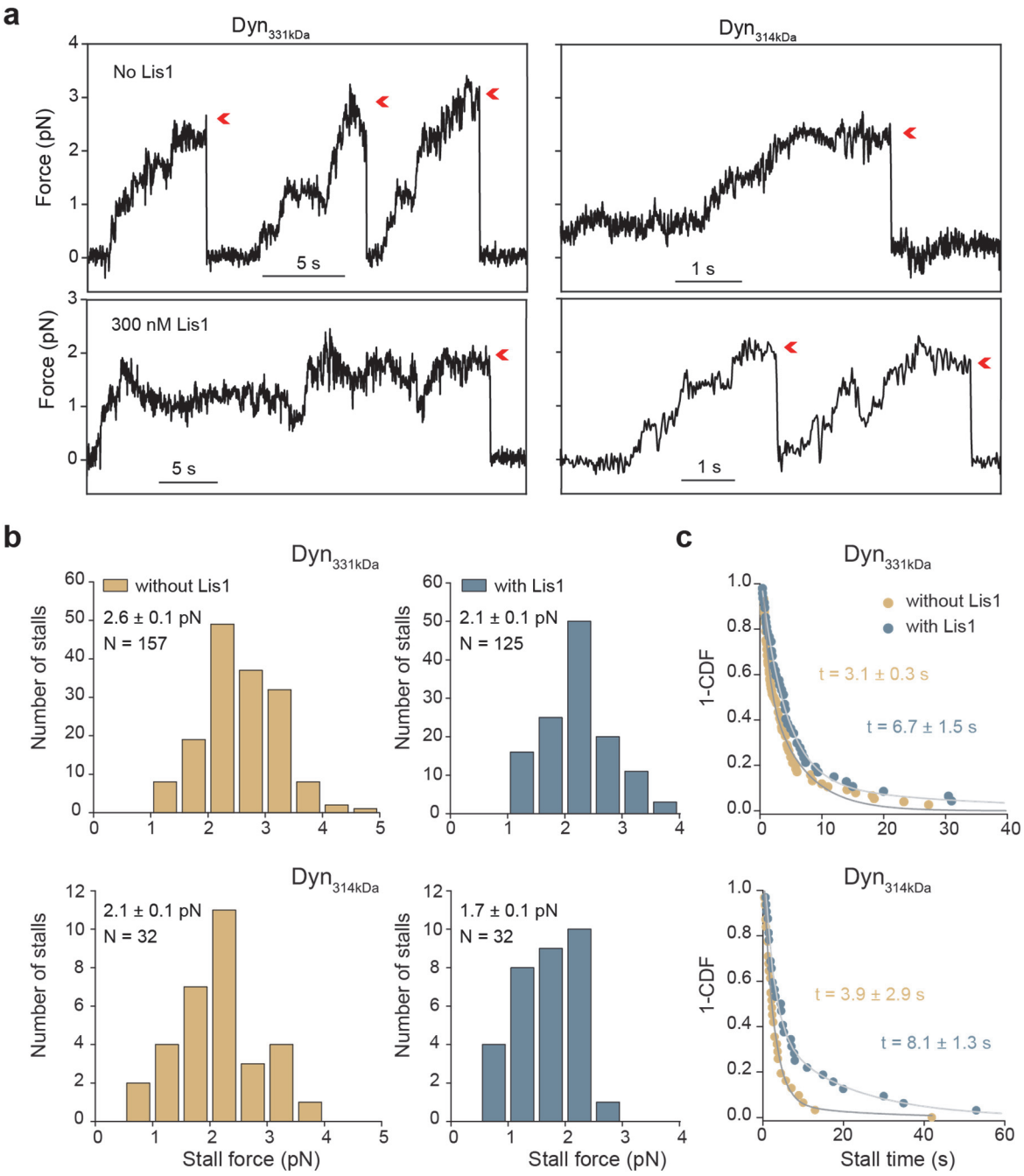

Extended Data Figure 7 | Lis1 reduces the stall force of the tail-truncated dynein. a) Representative trajectories of beads driven by GFP-GST-Dyn_{331kDa} and GFP-GST-Dyn_{314kDa} in the presence and absence of 300 nM Lis1. Red arrowheads represent the detachment of the motor from the microtubule followed by the snapping back of the bead to the trap center. **b)** Stall force histograms of Dyn_{331kDa} and Dyn_{314kDa} in the presence and absence of 300 nM Lis1 (mean ± s.e.m.; $p = 2x10^{-7}$ for Dyn_{331kDa} and 0.006 for Dyn_{314kDa}, two-tailed t-test). **c)** Stall durations of Dyn_{331kDa} and Dyn_{314kDa} in the presence and absence of 300 nM Lis1 ($p = 0.22$ and $p = 0.1$, respectively, Kolmogorov-Smirnov test). Fit to a double exponential decay (solid curves) reveals the average stall time (±s.e.).

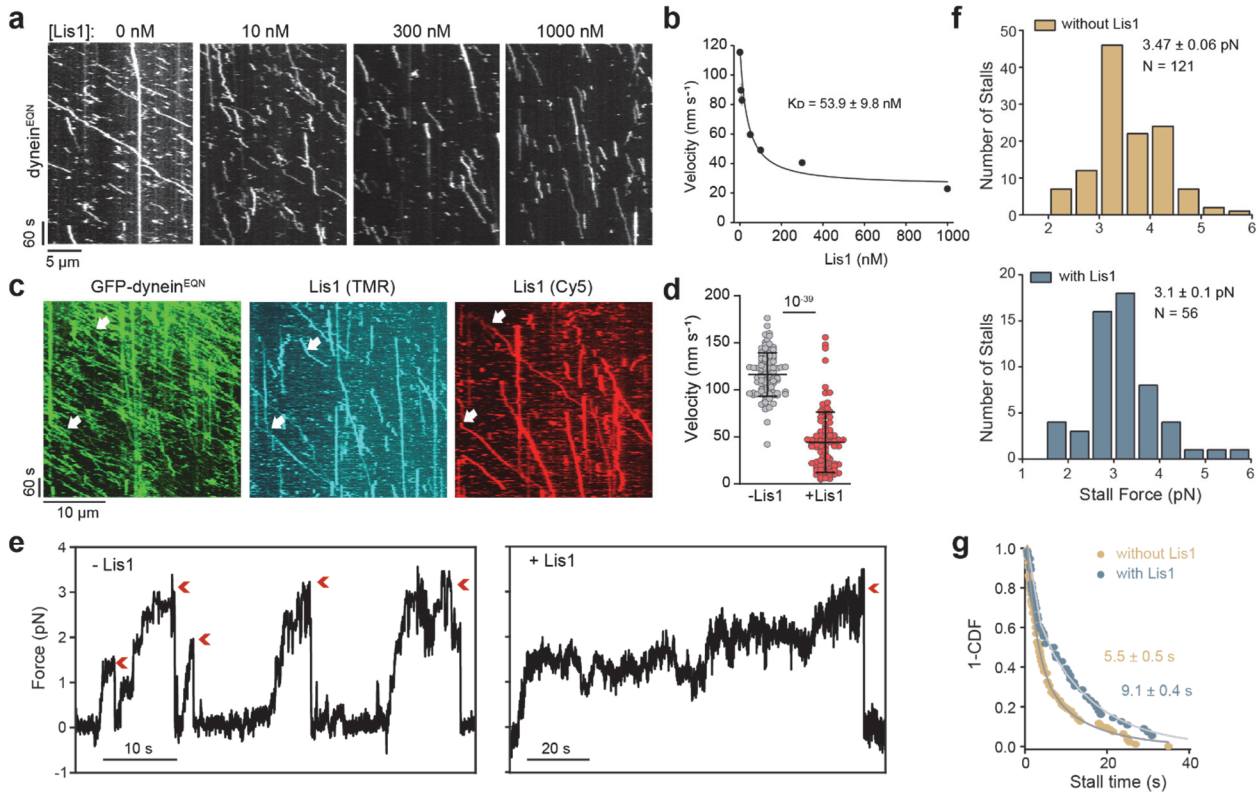

Extended Data Figure 8 | Lis1 binding to dynein's stalk is not required to slow down dynein motility. **a)** Representative kymographs of dynein^{EQN} motility under different concentrations of unlabeled Lis1. **b)** The velocity of dynein^{EQN} motility under different concentrations of unlabeled Lis1 (mean ± s.e.m.; N = 659, 283, 482, 484, 487, 610, 132 from left to right). The fit of the dynein^{EQN} velocity data (solid curve) reveals K_D (±s.e., see Methods). **c)** A representative kymograph of a three-color imaging assay shows two Lis1s to bind to the same dynein^{EQN} motor (white arrows). **d)** The velocities of dynein^{EQN} motors not colocalizing (-Lis1) or colocalizing (+Lis1) with Lis1 (N = 98 and 92 from left to right). The center line and whiskers represent the mean and s.d., respectively. The P-value was calculated by a two-tailed t-test with Welch correction. **e)** Representative trajectories of beads driven by dynein^{EQN} in the presence or absence of 900 nM Lis1. Red arrowheads represent the detachment of the motor from the microtubule followed by the snapping back of the bead to the trap center. **f)** Stall force histograms of dynein^{EQN} in the presence and absence of 900 nM Lis1 (mean ± s.e.m.; $p = 10^{-3}$, two-tailed t-test). **g)** Stall durations of dynein^{EQN} in the presence and absence of 900 nM Lis1. Fit to a double exponential decay (solid curves) reveals the average stall time (±s.e.).

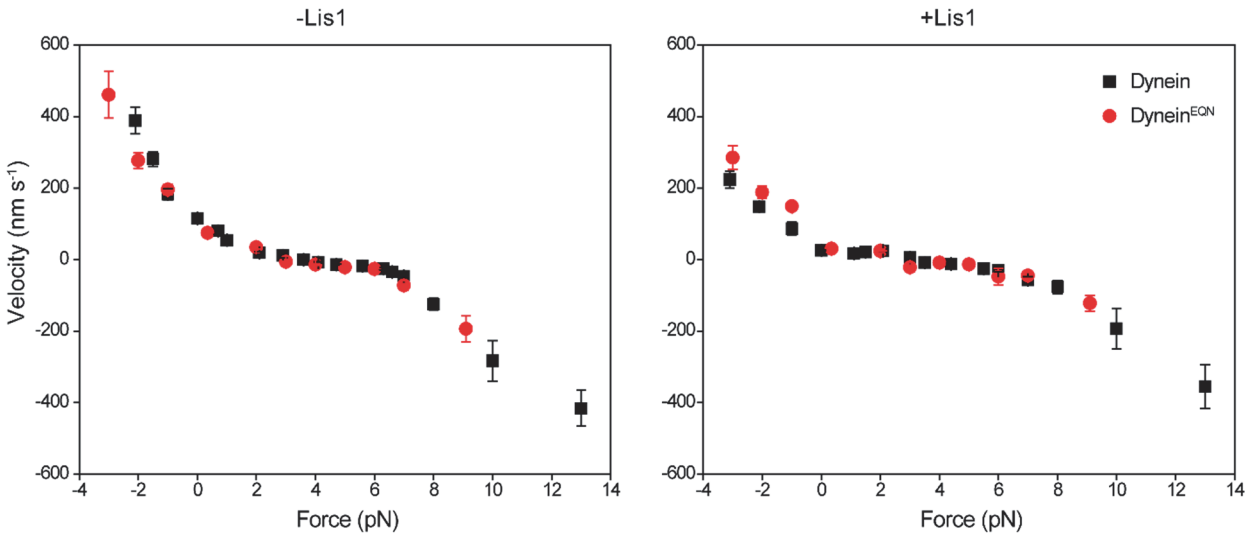

Extended Data Figure 9 | The comparison of the F-V behavior of dynein and dynein^{EQN} in the presence and absence of Lis1. (Left) F-V measurements of dynein and dynein^{EQN} in the absence of Lis1 (mean ±s.e.m., from left to right, N = 41, 38, 37, 861, 27, 52, 106, 28, 51, 60, 89, 115, 124, 62, 23, 38, 40 for dynein and N = 31, 66, 62, 48, 47, 26, 42, 39, 23, 45, 33 for dynein^{EQN}). (Right) F-V measurements of dynein in 300 nM Lis1 compared to F-V of dynein^{EQN} in 900 nM Lis1 (mean ±s.e.m., from left to right, N = 34, 52, 25, 312, 33, 42, 49, 37 62, 47 33 42, 36, 29, 18 for dynein; and N = 54, 36, 61, 31, 37, 17, 54, 14, 19, 38, 26 for dynein^{EQN}).